ARMY RESEARCH LABORATORY

Induction Heating of Carbon-Fiber Composites: Experimental Verification of Models

by Bruce K. Fink, Roy L. McCullough,
and John W. Gillespie, Jr.

ARL-TR-2247

June 2000

Army Research Laboratory
Aberdeen Proving Ground, MD 21005-5069

ARL-TR-2247 **June 2000**

Induction Heating of Carbon-Fiber Composites: Experimental Verification of Models

Bruce K. Fink
Weapons and Materials Research Directorate, ARL

Roy L. McCullough and John W. Gillespie, Jr.
University of Delaware

Abstract

Heating of continuous carbon-fiber-reinforced polymers (CFRP's) by the application of an alternating magnetic field has been shown to be due to dielectric losses in the polymer. Models that predict thermal generation in these composites are input to a finite element heat-transfer analysis, providing the predicted transient thermal profile in the plane of the laminate. The validity of the global thermal generation model is established through an experimental test matrix in which various specimen configurations are evaluated and compared with theoretical predictions of transient surface temperatures.

Table of Contents

INTENTIONALLY LEFT BLANK.

List of Figures

Page

List of Tables

INTENTIONALLY LEFT BLANK.

1. Introduction

A new theory of dielectric mechanisms for induction heating of continuous carbon-fiber composites was reported previously [1]. Based on these mechanisms, a global model was developed [2] that systematically defined the electromagnetic response of cross-ply laminated composites to alternating magnetic fields with some component of flux normal to the surface of the composite material. The global model consists of three fundamentally separate submodels that consider the in-plane electromagnetic response [3], the through-thickness response [4] and, finally, the global generation of heat and the quantification of the surface temperature profile presented in this paper. A thermal submodel is required for the comparison of predicted and measured temperatures at any point on the surface of a sufficiently thin laminated composite plate. Comparison of experimental with predicted surface temperatures can establish the validity of the postulated mechanisms of induction heating in continuous carbon-fiber composites.

Figure 1 shows an outline of the thermal submodel with the input parameters supplied by the foregoing submodels [1–5]. The planar grid submodel provides a two-dimensional (2-D) potential difference distribution for each ply-ply interface. The fiber layer submodel provides a key parameter γ describing the effective capacitive layer interaction distance and, thus, the profile of heating through the thickness for each orthogonal or off-axis ply-ply interaction in the laminate. These models can be combined to generate a three-dimensional (3-D) heat-source distribution in the laminate. In turn, this heat-source distribution can be used as input into a finite element heat-transfer model, which determines the surface thermal history of the laminate. This latter process is herein termed the "thermal submodel."

The predicted transient surface temperatures obtained from the thermal submodel are compared to experimental surface temperature measurements. ICI Fiberite's prepreg product APC-2 was used in the experimental studies. This material consists of ICI's poly-etheretherketone (PEEK) semicrystalline thermoplastic resin and continuous AS-4 graphite fibers.

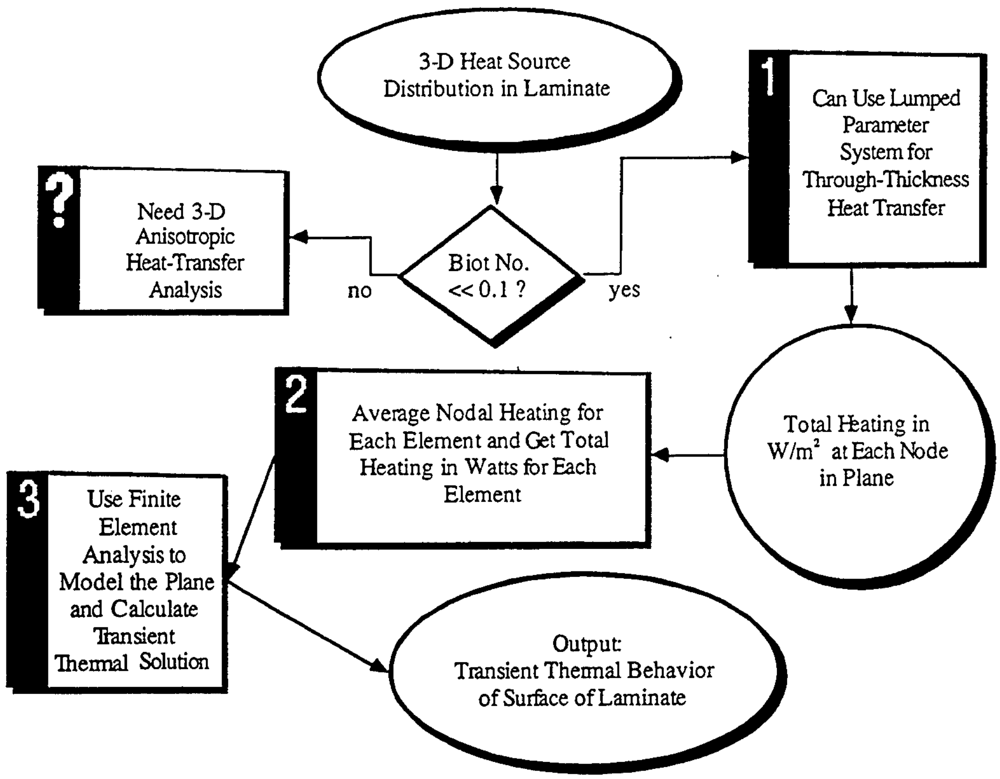

Figure 1. Outline of Thermal Submodel.

2. Thermal Conduction Considerations

The heating patterns in the plane, predicted by the planar grid submodel [2, 3], and those through the thickness, predicted by the fiber layer submodel [2, 4], combine to form a complex 3-D distribution of thermal generation in the laminate. Although the models can predict this energy generation point by point, it is difficult to translate these results into time-variant temperature distributions. Gradients in the plane can be accounted for through a discretization of the surface.

In general, a 3-D transient anisotropic ply-ply thermal analysis would be required. In our experiments, relatively thin laminates, where thermal gradients through the thickness are shown to be negligible, are studied to confirm the planar distribution of heating. To establish this fact, the through-thickness heat-transfer analysis considers the heat-generation profiles that were formulated in earlier work [2, 3], which can be somewhat complex. Each possible ply-ply interaction has such a profile and the resulting profile for a multi-ply laminate may consist of several extremum as illustrated in Figure 2.

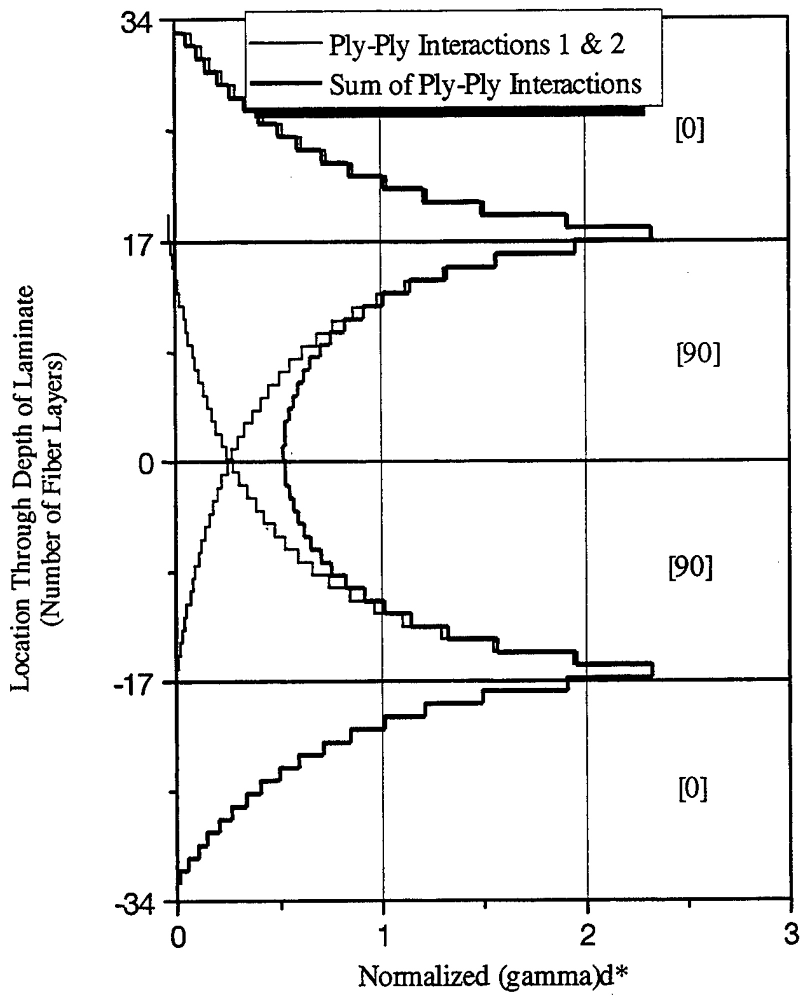

Figure 2. Superposition of Capacitive Layer Interaction Parameter, γd^*, Distributions for $[0/90_2]$ and $[90_2/0]$ Configurations. The Summation of These Distributions Provides the Gamma Distribution for the $[0/90]_S$ Configuration.

The profile within each ply can be represented by a third-order polynomial. Steady-state and transient solutions are obtained readily for a single ply-ply interaction using the equations of heating, $q(x)$, as a function of through-thickness dimension and a surface convection boundary condition. If the polynomial is of the form $a + bx + cx^2$ so that,

$$q(x) = \beta(a + bx + cx^2), \tag{1}$$

with

$$\beta = \frac{\omega\varepsilon_o\kappa\tan\delta V^2}{L}, \tag{2}$$

where ω is the angular frequency, ε_o is the permittivity of vacuum (8.85×10^{-12} f/m), κ is the relative dielectric constant of the polymer, $\tan\delta$ is the imaginary part of the complex dielectric constant of the polymer, V is the fiber-fiber interaction potential difference, and L is the characteristic dimension through which the electric field created by V acts [1]. The transient surface temperature can be written as

$$T(x,t) = T_x + \psi(x,t) + \Phi(x). \tag{3}$$

The term $\Psi(x,t)$ is the transient part of the solution, and $\Phi(x)$ is the steady-state part, viz.,

$$\Phi(x) = \frac{\beta}{k_{33}}\left[\frac{1}{2}a\left(L^2 - x^2\right) + \frac{1}{6}b\left(L^3 - x^3\right) + \frac{1}{12}c\left(L^4 - x^4\right)\right] + \frac{\beta}{h}\left[aL + \frac{1}{2}bL^2 + \frac{1}{3}cL^3\right], \tag{4}$$

where L is the half-thickness of the two-ply laminate, k_{33} is the thermal conductivity through the thickness, h is the combined convective and radiative heat-transfer coefficient, and x is the distance from the ply-ply interface toward the surface of the laminate. The transient part of the solution is written as

$$\Psi(x,t) = \sum_{n=1}^{\infty} A_n \cos\left(\frac{n\pi}{L}x\right)\exp\left(-\left(\frac{n\pi}{L}\right)^2\alpha^2 t\right), \tag{5}$$

with

$$A_n = \frac{-\beta}{2n\pi k_{33}}\left[aL + \frac{1}{2}bL^2 + \frac{1}{3}cL^3\right]. \tag{6}$$

The steady-state solution can be obtained independently in terms of the temperature at the surface, T_s:

$$T = T_s + \frac{h\theta}{k_{33}}(L-x) - \frac{\beta}{k_{33}}[\textit{fourth order polynomial in } x], \tag{7}$$

where

T_s = equilibrium temperature at the surface, and

$\theta = T_s - T_\infty$.

Using the previous equations and the parameters of Table 1, the maximum temperature difference in a representative laminate can be determined from both the transient and steady-state solutions. Figure 3 displays the results for the representative laminate at various time increments. For the transient solution, the largest difference in temperature between the ply-ply interface, T_o, and the laminate surface, T_s, occurs at small time. At time $t = 1$ s., this difference is approximately 5.6% of the surface temperature, T_s. At $t = \infty$, the transient solution is equivalent to the steady-state solution and the inside-to-outside difference is only 0.15% of the wall temperature.

Due to the time increments used in the experimental testing, 5–10 s, and the accuracy limitations of the equipment, temperature differences through the thickness are not measurable. Several tests were performed with thermocouples embedded at various points through the thickness of a $[0_3/125\text{-}\mu m\ \text{film}/90_3]$ laminate. No differences in temperature through the thickness were observed. In contrast, large variations in the plane are predicted enabling the verification of the planar grid model and the average heating through the thickness, $\int q(x)$.

Table 1. Input Parameters for the Representative Laminate Case Study. Some Values Are "Rational Estimates" for Determining the Maximum Possible Temperature Difference Within a Six-Ply Laminate, With an Interply Resin Thickness of $h_o = 127$ μm

Parameter	Symbol	Value	Dimension
Curve Fit Parameter	a	0.5169	1/m
Curve Fit Parameter	b	-1821.4	$1/m^2$
Curve Fit Parameter	c	1.484e6	$1/m^3$
See Equation (2)	β	23.32	W/m^2
Angular Frequency	ω	2π (70,000)	1/s
Emissivity Constant	ε_o	8.85e-12	f/m
Dielectric Constant	κ	3.6	dim.less
Loss Tangent	$\tan\delta$	0.16	dim.less
Maximum Voltage	V_{max}	68.0	V
Convection Coefficient	h	9.1	$W/m^{2\circ}C$
Thermal Conductivity	k_{33}	0.3	W/m°C
Ply Half-Thickness	L	4.445e-4	m
Coil Current	I	30	amp
Ambient Temperature	T_∞	25	°C

These results are also predicted by the Biot number, hL/k, and the rule-of-thumb that if Bi < 0.1, then a lumped-parameter analysis can be used since no significant temperature gradients exist through the material of characteristic dimension L. In this example for a six-ply laminate, the Biot number is approximately 0.012. Correspondingly, an APC-2 composite laminate would need to be greater than about 16 plies thick (i.e., approximately 0.2 cm or 0.08 in) before a more complex 3-D analysis would be required and appreciable differences in through-thickness temperature could be experimentally measured. The following section discusses how the output from the previous submodels is consolidated and used in a finite element program to model transient surface temperatures.

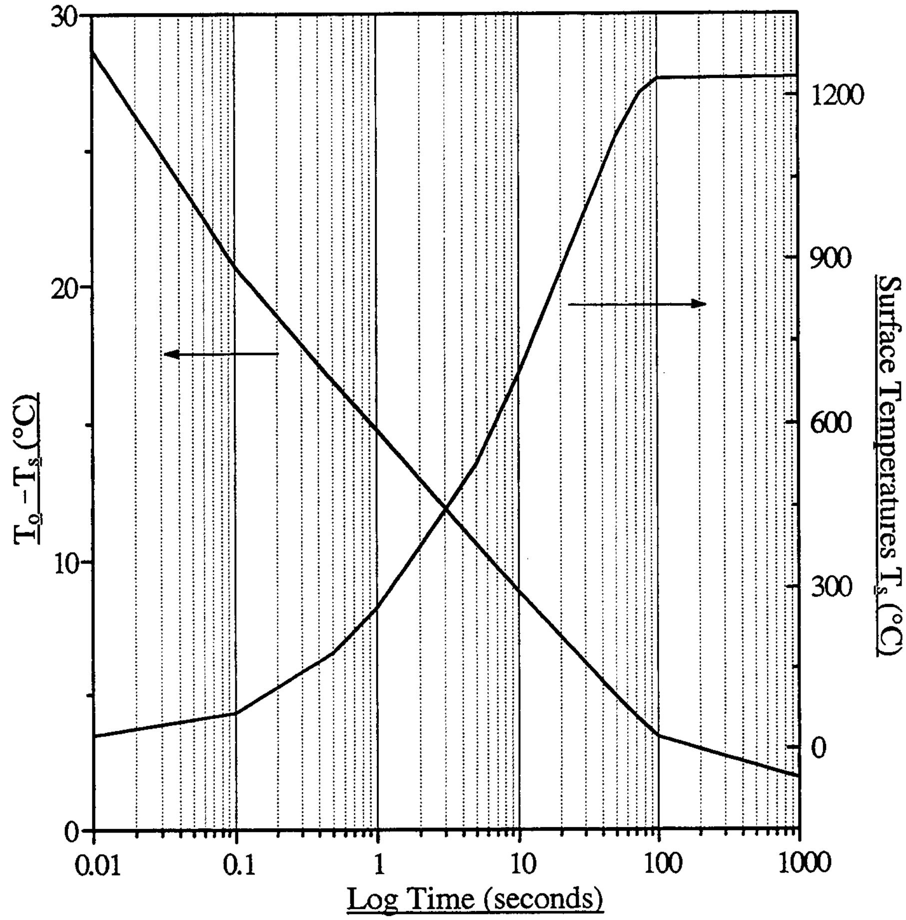

Figure 3. Results of Closed-Form 1-D Heat Transfer Solution for an Example Six-Ply Laminate. T_o is the Interface Temperature, and T_s is the Surface Temperature. Note That the Difference in Transient Temperature Between the Surface of the Specimen and the Center Is Negligible.

3. Elemental Heat Generation and Finite Element Heat-Transfer Solution

The desired input for the thermal model is the heat generation, q_{ij}, in the planar grid element (i,j) and its combined convective and radiative losses, h_{ij}. The nondimensional output of the planar grid submodel's program for node "r,s" is Λ_{rs}, where

$$\Lambda_{rs} = \frac{\upsilon_{rs}}{\omega\phi_B}. \tag{8}$$

The quantity υ_{rs} is the nodal voltage in volts at node (r,s), ω is the angular frequency, and ϕ_B is the magnetic flux in webers. The volume-normalized nondimensional output of the fiber layer submodel's program is Γ:

$$\Gamma = \frac{\gamma_{total} d^*}{b+n+m}, \tag{9}$$

where γ_{total} is the effective parameter of heating through the thickness of the laminate defined by the capacitive layer interaction calculations, d^* is the effective fiber layer separation distance, b is the ratio of the ply-ply separation distance h_o to the effective fiber layer separation distance d^* (i.e., $b = h_o/d^*$), and m and n are the number of fiber layers above and below the ply-ply interface respectively. The nondimensional parameters Λ_{rs} and Γ are used to obtain the total heating per element in the thermal model's grid. The grid used in the thermal model is equivalent to that used in the planar grid model. The nodal voltage in equation (8), υ_{rs}, can be solved for in terms of the program output, Λ_{rs}. Since the thermal model requires elemental heating values, the nodal voltages are averaged over the element they represent:

$$V_{ij} = \frac{1}{4}\left(\upsilon_{r,s} + \upsilon_{r,s+1} + \upsilon_{r+1,s} + \upsilon_{r+1,s+1}\right), \tag{10}$$

where V_{ij} is the elemental voltage for the element (i,j) of the models' grid (the commas are used only to separate the subscripts). The elemental heat generation in watts/cubic meter can now be written as,

$$q_{ij} = \omega\varepsilon_o\kappa\tan\delta\Gamma V_{ij}^2, \tag{11}$$

where the imaginary part of the complex dielectric constant, $\tan\delta$, is a function of temperature [2]. From these procedures, the quantity X_{ij} can be obtained:

$$X_{ij} = \frac{q_{ij}}{\tan\delta}, \tag{12}$$

with X_{ij} in watts/cubic meter.

The finite element analysis (FEA) program FEHT was used for the heat-transfer analysis. A 7×7 element grid was used as illustrated in Figure 4. A grid size of 7×7 is accurate for centered-coil tests in which the coil's flux area covers at least 14% of the surface of the specimen as determined by a convergence study for the planar grid model [2], with an error of about 7% from the infinitely fine grid. This grid size was the maximum size that could be used for the experimental arrangement described in the following section. It represents a practical choice in terms of computer time limitations, geometric feasibility, and sufficient surface temperature measurement accuracy for comparison to the predicted transient surface temperature profile. Each of the 49 planar grid model elements from $(i,j) = (1,1)$ to $(7,7)$ were broken up into eight FEA elements, for a total of 392 FEA elements, and 225 FEA nodes.

Figure 5 shows how each square model element was partitioned into its FEA elements. The quantity X_{ij} from equation (12) represents the thermal generation in the model element (i,j). X_{ij} has a gradient over the model element area. This gradient can be calculated from the original υ_{rs} quantities output from the ply-ply interaction model as defined in equation (8). The gradients between the four nodal υ_{rs} quantities for each model element are assumed to be linear so that the heating for each FEA element can be calculated through a simple linear regression involving the nodal voltage parameters υ_{rs} and X_{ij}. Figure 5 defines the nodal locations "a" through "d" in addition to the υ_{rs} nodes.

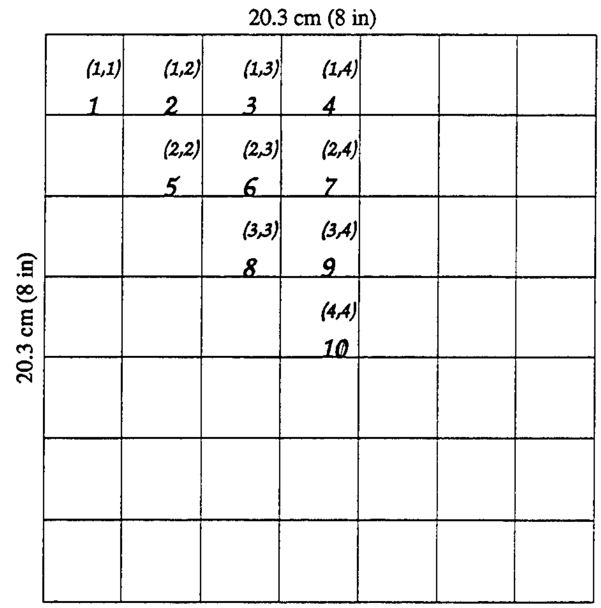

Figure 4. Grid Used in Final Experimental Test Matrix. The Planar Grid Element Labeled 1–10 Represent the Entire Surface Due to Symmetry in the Cross-Ply Specimen and in the Central Placement of the Coil.

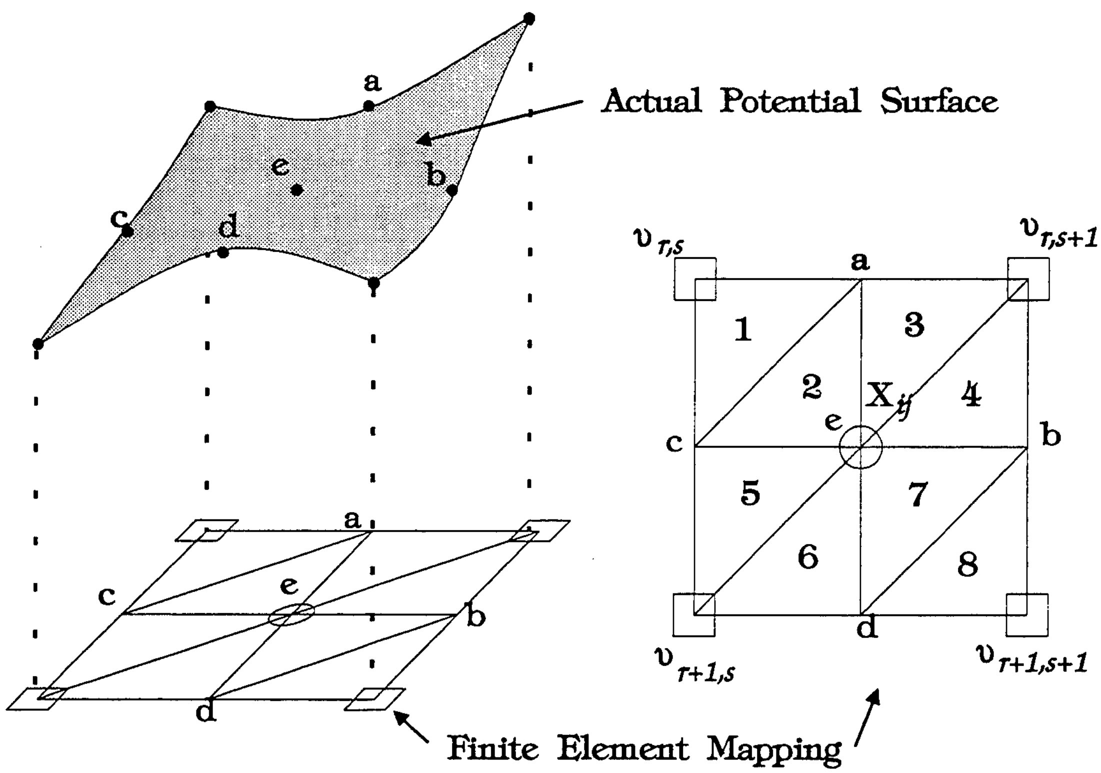

Figure 5. Mapping From Voltage Surface to Finite Element Model Nodes.

Assuming linear gradients along the edges, the nodal heating values at all nodes can be calculated as

$$a_{ij} = \frac{\mathrm{X}_{ij}}{V_{ij}}\left[\upsilon_{r,s} + \frac{\upsilon_{r,s+1} - \upsilon_{r,s}}{2}\right],$$

$$b_{ij} = \frac{\mathrm{X}_{ij}}{V_{ij}}\left[\upsilon_{r,s+1} + \frac{\upsilon_{r+1,s+1} - \upsilon_{r,s+1}}{2}\right],$$

$$c_{ij} = \frac{\mathrm{X}_{ij}}{V_{ij}}\left[\upsilon_{r,s} + \frac{\upsilon_{r+1,s} - \upsilon_{r,s}}{2}\right], \text{ and}$$

$$d_{ij} = \frac{\mathrm{X}_{ij}}{V_{ij}}\left[\upsilon_{r+1,s} + \frac{\upsilon_{r+1,s+1} - \upsilon_{r+1,s}}{2}\right]. \tag{13}$$

The eight FEA element heating values per grid element (i,j) are given by

$$\mathrm{X}_{ij,1} = \frac{1}{3}\left[\frac{\mathrm{X}_{ij}}{V_{ij}}\upsilon_{r,s} + a_{ij} + c_{ij}\right],$$

$$\mathrm{X}_{ij,2} = \frac{1}{3}\left[\mathrm{X}_{ij} + a_{ij} + c_{ij}\right],$$

$$\mathrm{X}_{ij,3} = \frac{1}{3}\left[\frac{\mathrm{X}_{ij}}{V_{ij}}\upsilon_{r,s+1} + \mathrm{X}_{ij} + a_{ij}\right],$$

$$\mathrm{X}_{ij,4} = \frac{1}{3}\left[\frac{\mathrm{X}_{ij}}{V_{ij}}\upsilon_{r,s} + \mathrm{X}_{ij} + b_{ij}\right],$$

$$\mathrm{X}_{ij,5} = \frac{1}{3}\left[\frac{\mathrm{X}_{ij}}{V_{ij}}\upsilon_{r+1,s} + \mathrm{X}_{ij} + c_{ij}\right],$$

$$X_{ij,6} = \frac{1}{3}\left[\frac{X_{ij}}{V_{ij}}\upsilon_{r+1,s} + X_{ij} + d_{ij}\right],$$

$$X_{ij,7} = \frac{1}{3}\left[X_{ij} + b_{ij} + d_{ij}\right], \text{ and}$$

$$X_{ij,8} = \frac{1}{3}\left[\frac{X_{ij}}{V_{ij}}\upsilon_{r+1,s+1} + b_{ij} + d_{ij}\right]. \tag{14}$$

The average of $X_{ij,1}$ through $X_{ij,8}$ is not exactly equal to X_{ij} due to the assumption of linear gradients between adjacent nodes; however, this error was consistently less than the 7% error inherent in the planar grid analysis for the specimens modeled and tested. For the centered-coil tests used, some model elements, (i,j), had equivalent heat-generation input values. Due to this symmetry, 10 distinct input values were possible, as shown in Figure 4. The "heat generation" term needed for the thermal calculation is

$$q_{ij,k} = \tan\delta(T) - \frac{2h_{ij,k}(T)}{L}, \tag{15}$$

where

$q_{ij,k}$ = total heat flux in FEA element k of model element (i,j),

$X_{ij,k}$ = output after linear regression fits,

$\tan\delta(T)$ = dielectric loss tangent as a function of element temperature,

$h_{ij,k}$ = combined convective and radiative heat transfer losses from each surface of the plate as a function of element temperature, and

$L = (b + m + n)d^*$ = thickness of plate.

The two fundamental parameters, $\tan\delta(T)$ and $h_{ij,k}(T)$, were experimentally investigated. A study of the loss tangent properties of PEEK was performed and is presented, in detail, in Fink [2] and Fink, McCullough, and Gillespie [5]. The convection heat transfer coefficient, h, was experimentally determined for the test configuration. This analysis is discussed in Fink [2].

Other input to the program includes the density, heat capacity and thermal conductivity of the material. The FEA program requires the input of effective quasi-isotropic thermal properties. The thermal conductivity of an APC-2 prepreg ply is highly anisotropic; the value in the fiber direction, k_{11}, is approximately 6.20 W/m°C, and, in the transverse direction, k_{22}, is approximately 0.34 W/m°C from fiber volume fraction calculations using polymeric and anisotropic fiber properties (Table 2) and a fiber volume fraction of 0.61. For orthotropic cross-ply laminates in which the number of 0° plies is equal to the number of 90° plies (M = N), isotropic values for thermal conductivity can be used.

Table 2. Material Properties for Poly-Etheretherketone and AS-4 Carbon Fibers

	Specific Heat J/kg°C	Density kg/m^3	Thermal Conductivity W/m°C
Matrix (PEEK) [6]	1,340	1,320	0.2512
Fiber (AS-4 Graphite) [8]	921	1,800	0.426 (trans.) 10.0 (long.)

Consider a $[0_M/h_o\_thick\_film/90_N]$ cross-ply laminate consisting of M 0° plies, an interlayer resin thickness of h_o, and N 90° plies. A "longitudinal" value for the thermal conductivity, k_L, of the laminate can be estimated through volume averaging:

$$k_L^{laminiate} = \frac{Mk_{11}^{ply} + Nk_{22}^{ply} + \dfrac{h_o}{127}k_m}{M + N + \dfrac{h_o}{127}}, \tag{16}$$

where

k_m = thermal conductivity of matrix ≈ 0.2512 W/m°C, and

h_o is measured in microns.

For $M = N = 1$ and $h_o = 8$ μm (a normally consolidated [0/90] cross-ply laminate), k_L for the laminate is approximately 3.18 W/m°C. For balanced laminates, $M = N$, the longitudinal and transverse conductivities are equivalent, $k_L = k_T$. As long as thermal gradients through the thickness are minimal, the in-plane thermal conductivity is isotropic. Similar calculations are possible for determining the density, ρ, and specific heat, c_p, values for the various configurations under consideration.

4. Experimental Procedures

The thermal submodel described previously completes the global model of heating in cross-ply, continuous carbon-fiber-reinforced composites. The local, in-plane, and through-thickness submodels are combined to provide input to a finite element heat-transfer analysis, providing the predicted transient thermal profile in the plane of thin laminates. Error calculations concerning through-thickness thermal gradients and linearity of potential field gradients in the plane were considered in the solution. As shown later, the validity of the assumptions that encompass the thermal submodel are supported by the close agreement with the model's output with experimental data.

The following sections provide experimental evidence supporting the global model. The various submodels previously discussed [1–5] established the significant physical parameters required to characterize the response of cross-ply composites to alternating magnetic fields. Various material and experiment-related quantities are evaluated individually and tabulated with their corresponding errors. An experimental test matrix was performed that represents a practical range of the significant parameters and the effects of changing those parameters individually.

Table 3 shows the 20.3-cm-square (8 in) plate lay-up configurations fabricated and tested using coil currents of 6, 10, and 20 amp; the matrix consists of 75 separate tests. The placement of the 10 surface thermocouples is shown in Figure 4. Specimens were labeled as indicated in Table 3 and are referred to by the codes shown in parentheses, e.g., (0_11) represents the 0-mil interlayer $[0_1/90_1]$ specimen and (5_22) represents the 5 mil interlayer $[0_2/90_2]$ laminate specimen where 1 mil = 25.4 μm. Specimens are further referred to as, for example, (0_11_6), where the "6" represents the coil current used in amps.

Table 3. Laminate Configurations Processed for Final Test Matrix. Each 20.3-cm-Square (8 in) Specimen Was Tested With a 10.2-cm-Diameter (4 in) Centered Helmholtz-Type Coil at 6-, 10-, and 20-amp Applied Coil Current.

		Nominal Interlayer PIIK Resin Film Added, h_o (1 mil = 25.4 μm)				
		(None)	1 mil	2 mil	3 mil	5 mil
	(1,1)	A (0_11)	B (1_11)	C (2_11)	D (3_11)	E (5_11)
	(2,2)	F (0_22)	G (1_22)	H (2_22)	I (3_22)	J (5_22)
(M,N)	(3,3)	K (0_33)	L (1_33)	M (2_33)	N (3_33)	O (5_33)
	(1,2)	P (0_12)	Q (1_12)	R (2_12)	S (3_12)	T (5_12)
	(1,3)	U (0_13)	V (1_13)	W (2_13)	X (3_13)	Y (5_13)

DuPont Co. provided the use of an Ameritherm 50–200-kHz 15-kW induction generator. The machine self-tunes the frequency for the coil and load placed on it. Output includes the frequency, current to coil, and voltage applied. The current to the coil reading has about a 2-amp error in the reading itself, which can be 100% of the total reading when applying low power to the coil. The induction coils were fabricated using 1/4-in-outside-diameter. Copper tubing and compression fittings using a Helmholtz design, which provides a very uniform field with all field lines normal to the plane of the specimen and with constant flux across the plane of the specimen. The coil design used in our experiments tunes to the Ameritherm equipment at 70 kHz. The 20.3-cm-square (8 in) specimens were placed in a wooden frame, which serves two purposes. First, it grips the specimen along all four edges (with 1/8-in overlap at the edges) and keeps the unbalanced (1,2) and (1,3) and the unsymmetrical laminates (all specimens) square in the plane. Second, the frame assembly slides vertically between two grooved wooden guides attached to a wooden base, allowing the frame and, thus, the specimen to be rapidly dropped into the stationary Helmholtz coil position. This provides an instant-on capability for the field not otherwise possible with the Ameritherm induction equipment at such low coil-currents, due to the self-tuning nature of the equipment. The thermocouples were placed on the specimen and each read by a digital E-type thermocouple reader (a computerized input was not available). The accuracy of these readers is ±1 °C. The process, including the thermocouple readers and a digital timer, was recorded on videotape, which was later reviewed to record the thermocouple readings at 10-s increments. These time increments provided sufficient accuracy for comparison to predictions.

5. Model Predictions

Table 4 indicates the values used in the models for comparison with the final experimental matrix. The application of the predictive models is illustrated for the laminate configuration (0_11_6). Nondimensional laminate and induction source parameters (generally, those without error values) were input into the planar grid in-plane interaction submodel, providing a dimensionless nodal voltage matrix. Separately, dimensional laminate characteristics and their respective errors were input to the fiber layer through-thickness interaction submodel, providing the total effective inverse fiber-layer interaction distance per unit thickness. These outputs were combined with additional material and laminate properties for input into a program based upon the local and in-plane interaction submodels. This output provides the 7×7 heat-generation matrix per unit loss tangent with upper and lower error bounds. These results were then used as input to the 2-D FEA heat-transfer submodel along with loss tangent and surface heat-loss functions with temperature to provide the predicted transient thermal behavior at the surface of the laminates.

Table 4. Values and Associated Errors for Material and Experimental Parameters

Property	Symbol	Source	Value	Error	Units
Coil Current	I	Machine Reading	6, 10, 20	± 2	Amps
Magnetic Flux	ϕ_B	Coil Calc's [2]	1.219e-6*I	Lo: 1.08e-6*I Hi: 1.219e-6*I	Webers
Frequency	f	Machine Reading	70,000	± 2000	Hertz
Dielectric Constant	ε	Measured [5]	3.72	± 0.10	dim.less
Dielectric Loss Tangent	$\tan \delta$	Measured [5]	Varies With T [2]	3 % [2]	dim.less
Fiber Diameter	df	[8]	8	± 0.5	microns
Fiber Volume Fraction	X_f	[9]	0.61	± 0.01	dim.less
Radiation Heat-Transfer Losses	R	Estimated [2]	Varies With T [2]	N/A	$W/m^2°C$
Number of Fiber Layers Per Ply	m/M,n/N	Measured [2]	17.3	± 1.6	dim.less
Actual Interply Thickness Per Unit Nominal Input	ho/Nom. Input	Measured [2]	0.840 Except for 0-mil Specimen	0.065 Except for 0-mil Specimen	dim.less
Total Laminate Thickness	2L	Calculated	Varies With Specimen	Varies With Specimen	meters
Wall Temperature	Ts	Measured	Varies (Depends on Rate)	± 1	°C
Convective Heat-Transfer Coefficient	h	Measured [2]	9.1	± 0.1	$W/m^2°C$
Heat Capacity	c_p	Calculated	[2]	N/A	J/k°C
Density	ρ	Calculated	[2]	N/A	kg/m^3
Thermal Conductivity	k	Calculated	[2]	N/A	W/m°C

Equation (17) is the input unit magnetic flux matrix for the planar grid model (the total input sums to unity). This input best represents the shape and placement of the coil and the distribution of flux on the surface for a 7×7 grid. Note that, although the distribution of flux is continuous in the actual laminate plane, the coarse modeled grid of the planar grid model necessarily has some partially filled elements as has been previously established [2].

$$\frac{[\phi_B]}{\sum_{j=1}^{7}\sum_{i=1}^{7}\phi_{B_{ij}}} = \begin{bmatrix} 0 & 0 & 0 & 0 & 0 & 0 & 0 \\ 0 & 0 & 0 & 0 & 0 & 0 & 0 \\ 0 & 0 & 0.071 & 0.143 & 0.071 & 0 & 0 \\ 0 & 0 & 0.143 & 0.143 & 0.143 & 0 & 0 \\ 0 & 0 & 0.071 & 0.143 & 0.071 & 0 & 0 \\ 0 & 0 & 0 & 0 & 0 & 0 & 0 \\ 0 & 0 & 0 & 0 & 0 & 0 & 0 \end{bmatrix}. \tag{17}$$

Equation (18) displays an example of the 8×8 matrix of dimensionless nodal voltage (i.e., voltage per unit frequency per unit flux) for the (0_11_6) laminate analysis. The nondimensionalized total effective inverse interaction distances, γ, for the predicted parameters and their errors (Table 4) for each specimen type (and 10-mil [254 μm] interlayer thickness) were determined previously [2].

$$\Lambda_{rs} = \left[\begin{array}{cccc:cccc} 0.757 & 0.840 & 0.943 & 0.426 & 0.426 & 0.943 & 0.840 & 0.757 \\ 0.840 & 0.943 & 1.08 & 0.490 & 0.490 & 1.08 & 0.943 & 0.840 \\ 0.943 & 1.08 & 1.27 & 0.581 & 0.581 & 1.27 & 1.08 & 0.943 \\ 0.426 & 0.490 & 0.081 & 0.175 & 0.175 & 0.081 & 0.490 & 0.426 \\ \hdashline 0.426 & 0.490 & 0.081 & 0.175 & 0.175 & 0.081 & 0.490 & 0.426 \\ 0.943 & 1.08 & 1.27 & 0.581 & 0.581 & 1.27 & 1.08 & 0.943 \\ 0.840 & 0.943 & 1.08 & 0.490 & 0.490 & 1.08 & 0.943 & 0.840 \\ 0.757 & 0.840 & 0.943 & 0.426 & 0.426 & 0.943 & 0.840 & 0.757 \end{array}\right]. \tag{18}$$

Note in equation (18) that the dotted lines delineate symmetry about the one-eighth section. In the equations that follow, this symmetry is noted.

Several observations derived from parametric studies are useful in predicting the trends of through-thickness heating as a function of the number of plies (M,N) on either side of the interface and of the thickness of the matrix-rich interface, h_o. Figure 6 shows the effect of increasing M for various nominal values of h_o (data is shown without error bars for ease of reading). Note that the effect (i.e., the change in heating with increasing M) is greater for larger interface thicknesses due to the dominance of the parameter h_o. Figure 7 shows the effect of increasing h_o for the various laminate configurations. Note that the (1,2) and (1,3) configurations do not differ significantly in heating and that the (1,3) and (2,2)—each with equivalent numbers of plies—heat significantly differently; both of these observations are due to the ineffectiveness of increasing the number of plies on one side of the interface. Finally, it is of interest to compare the predicted overall "heating" of the fiber layer interaction model with a situation in which dielectric heating is restricted to the interface region, h_o. Figure 8 compares the nondimensionalized "effective" inverse interaction distances from the present model with the nondimensionalized inverse h_o (note the inverse x-axis scale to represent increasing interface thickness). As the interface thickness gets larger (i.e., inverse h_o approaches zero), the difference between the two models approaches zero since h_o dominates the heating at low values. However, at practical interface thicknesses (even for specimens with no additional PEEK interlayer film), the present model predicts heating that is 2–3 orders of magnitude higher than the situation in which heating occurs only at the interface.

The planar voltage profile of equation (18) and the total effective through-thickness interaction parameter, γ, were used to predict the heating profile in the plane of the specimen in watts/cubic meter per unit loss tangent as shown in equations (19a–c). "B" represents the predicted values, while "U" and "L" represent the upper and lower bounds calculated from the values and errors tabulated in Table 4.

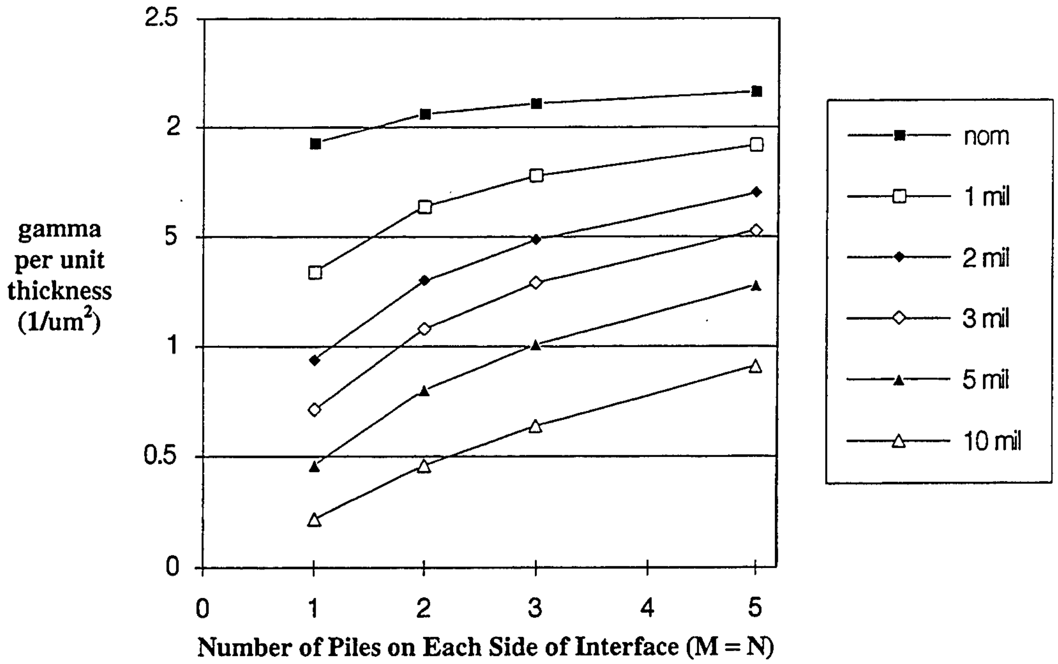

Figure 6. Predictions of Capacitive Layer Model Study of Test Matrix Specimens Showing the Effect of Increasing Ply Thickness on Heating.

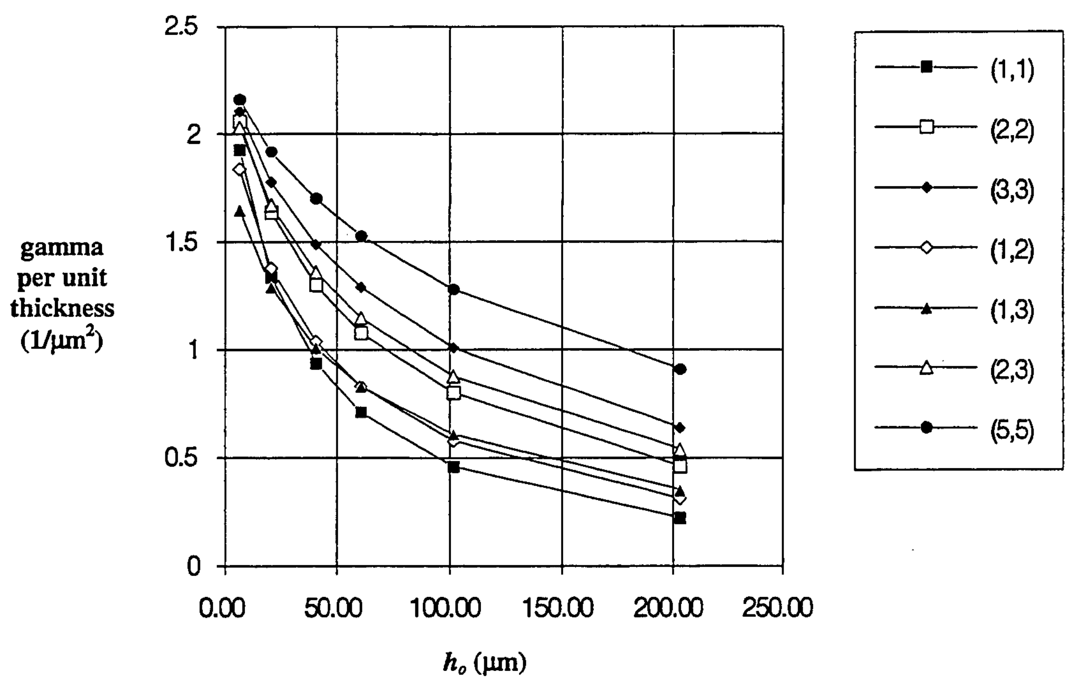

Figure 7. Predictions of Capacitive Layer Model Study of Test Matrix Specimens Showing the Effect of Increasing Interface Thickness on Heating.

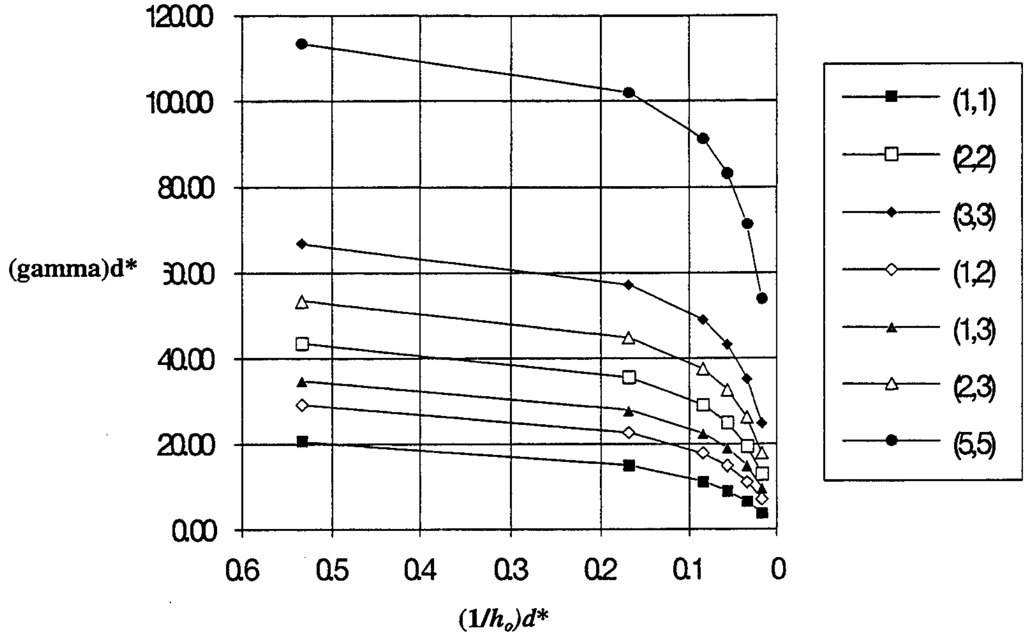

Figure 8. Predictions of Capacitive Layer Model Study of Test Matrix Specimens Comparing Nondimensional "Effective" Inverse Interaction Distances With the Nondimensionalized h_o. Note the Inverse x-Axis Scale to Represent Increasing Interface Thickness.

$$Q_B = \begin{bmatrix} 14.7 & 18.6 & 11.1 & 4.31 & & \\ & 24.5 & 15.0 & 5.90 & & \\ & & 8.71 & 2.94 & & \\ \text{sym.} & & & 0.627 & & \\ & & & & \text{sym.} & \\ & & & & & \end{bmatrix} \times 10^6 \ \frac{\mathrm{W}}{\mathrm{m}^3}, \qquad (19a)$$

$$Q_U = \begin{bmatrix} 23.0 & 29.2 & 17.4 & 6.76 & & \\ & 38.4 & 23.5 & 9.25 & & \\ & & 13.6 & 4.60 & & \\ \text{sym.} & & & 0.982 & & \\ & & & & \text{sym.} & \\ & & & & & \end{bmatrix} \times 10^6 \ \frac{\mathrm{W}}{\mathrm{m}^3}, \text{ and} \qquad (19b)$$

$$
Q_L = \begin{bmatrix} 7.06 & 8.94 & 5.33 & 2.07 & & & \\ & 11.8 & 7.21 & 2.84 & & & \\ & & 4.18 & 1.41 & & & \\ \text{sym.} & & & 0.030 & & & \\ & & & & & & \\ & & & & & \text{sym.} & \\ & & & & & & \end{bmatrix} \times 10^6 \ \frac{W}{m^3}. \qquad (19c)
$$

Note that the symmetrical placement of the coil on the specimen and the circular shape of the coil leads to only 10 unique values in the matrix Q. The 325% increase in heating from the lower bound to the upper bound appears substantial. However, this difference translates into only a 15 °C difference in surface temperature at the hottest point on the surface, as shown in Figure 9.

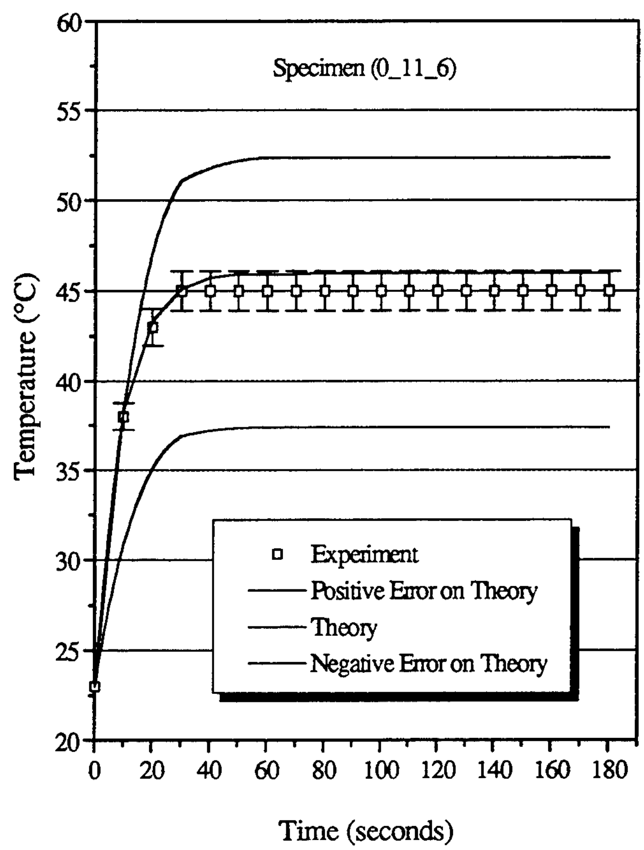

Figure 9. Experimental Surface Temperature History for Thermocouple No. 5 on (0_11_6) Test Specimen.

Equations (20a–c) show the predicted surface temperature profile and the corresponding upper and lower bounds respectively.

$$T_B = \begin{bmatrix} 33.9 & 38.4 & 31.4 & 25.3 & & \\ & 46.0 & 35.0 & 26.0 & & \\ & & 29.1 & 23.8 & & \\ \text{sym.} & & & 23.0 & & \\ & & & & & \\ & & & & \text{sym.} & \\ & & & & & \end{bmatrix} {}^\circ\text{C}, \tag{20a}$$

$$T_U = \begin{bmatrix} 36.0 & 41.8 & 32.8 & 25.8 & & \\ & 52.4 & 37.7 & 26.2 & & \\ & & 30.5 & 24.0 & & \\ \text{sym.} & & & 23.0 & & \\ & & & & & \\ & & & & \text{sym.} & \\ & & & & & \end{bmatrix} {}^\circ\text{C}, \text{ and} \tag{20b}$$

$$T_L = \begin{bmatrix} 29.9 & 32.9 & 28.5 & 24.6 & & \\ & 37.4 & 30.8 & 25.3 & & \\ & & 27.2 & 23.7 & & \\ \text{sym.} & & & 23.0 & & \\ & & & & & \\ & & & & \text{sym.} & \\ & & & & & \end{bmatrix} {}^\circ\text{C}. \tag{20c}$$

Large differences between the theoretical bounds in surface temperature were common; especially for the lower currents. In addition to the large machine-induced error in current readings, other factors add to the disparity in the bounds of the thermal response. The sensitivity of the microstructural properties of fiber diameter and fiber volume fraction and the macrostructural properties of interply resin-rich region thickness and average number of fibers through the thickness of a single ply have significant effects on the predicted bounds. However, experimental results are later shown to verify the predicted solution despite the wide bounds. This is due to the averaging of these properties over millions of actual nodal locations (fiber-fiber intersections), which tends to smooth out the effects of any deviations from the average in these structural properties.

6. Comparison of Predicted and Observed Temperature Profiles

Although experimental results for the nonorthotropic laminates [e.g., (1,2) and (1,3)] were obtained [2], comparable theoretical results were not feasible due to the FEA program's inability to handle anisotropic thermal conductivity properties. Accordingly, attention is directed to the orthotropic laminates (1,1), (2,2), and (3,3). The model results are obtained from the FEA nodal transient temperatures for the 10 nodes corresponding to the thermocouple locations, as shown previously in Figure 4. Only the results for the 10-amp applied coil-current tests are considered here. This current resulted in significant heating for all specimens, while remaining under the melting temperature of PEEK and, more importantly, within the range of temperatures for which the loss tangent was measured. The (0_11_6) specimen is examined in detail. Fink [2] presents extensive additional data for other specimens.

6.1 Planar Temperature. Figure 10 shows the experimental transient surface temperature results over the first 3 min. As noted previously, Figure 9 shows the predicted results for the point of highest heating on the surface of the specimen with the experimental results for the point of highest heating superimposed with the appropriate error bars. The equilibrium experimental value is 45 °C, while the theoretical equilibrium value is 46 °C, representing a (1/(46-23))x100 = 4% decrease in temperature gain. Figure 11 compares the equilibrium results for all thermocouples with the corresponding predicted values. Note that the No. 2 and No. 6 thermocouple positions heated more than the theory predicted, while the No. 1 and No. 3

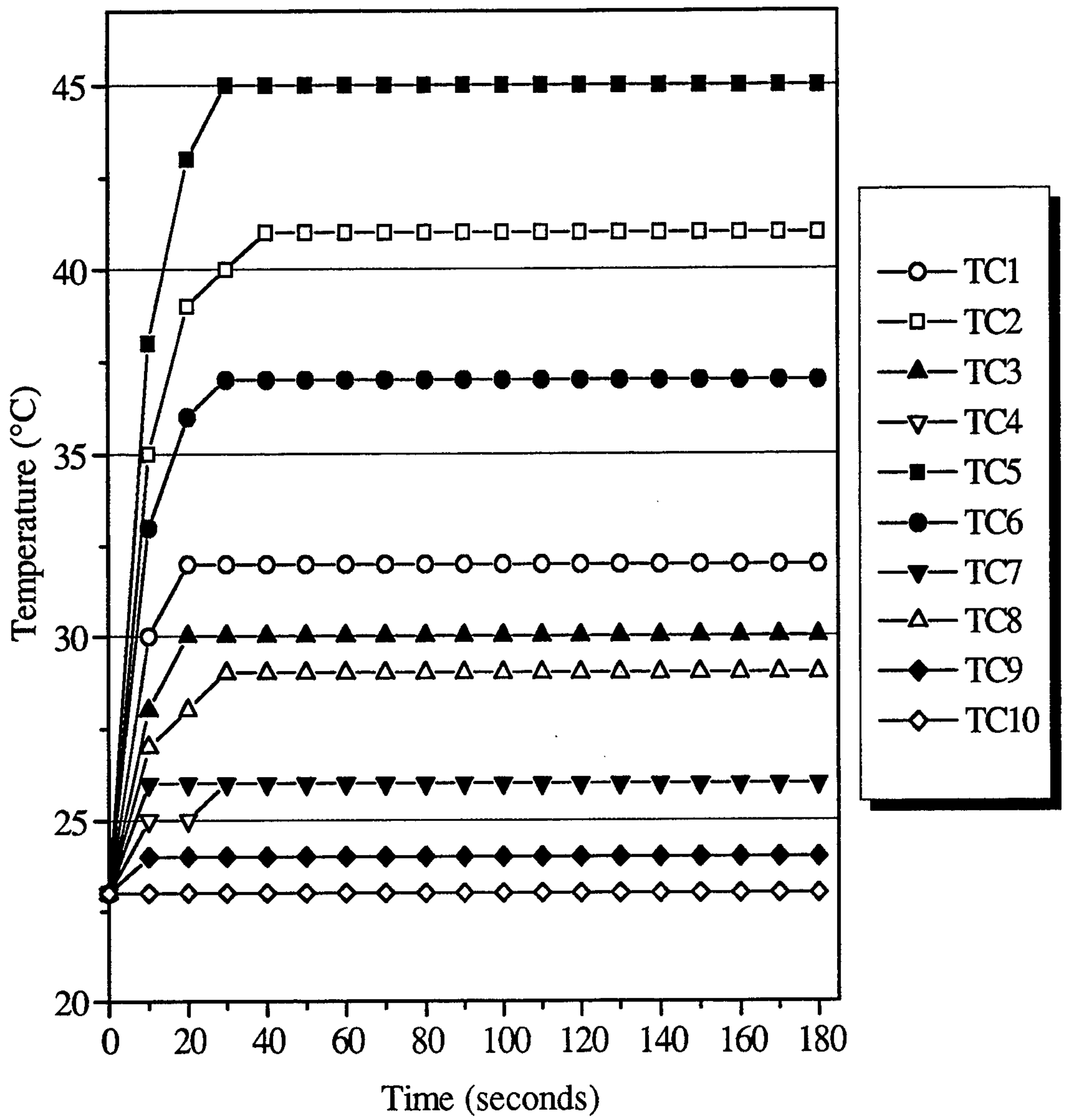

Figure 10. Experimental Transient Surface Temperature Results for Specimen (0_11_6) for All Nodal Positions.

positions heated less than the model predicted. Figure 12 indicates the thermocouple positions on the specimen and the percent difference of observed and predicted equilibrium temperature averaged over all the 10-amp tests and normalized against the ratio of experimental to predicted equilibrium surface temperature for position No. 5. The standard deviation in these results was less than 2%. Note, again, the significant increase in the No. 2 and No. 6 positions and the slight decrease in the No. 1, No. 3, and No. 8 positions. This expected result is explained by the 1-D assumption and the analysis of effective properties in which individual plies are not modeled in

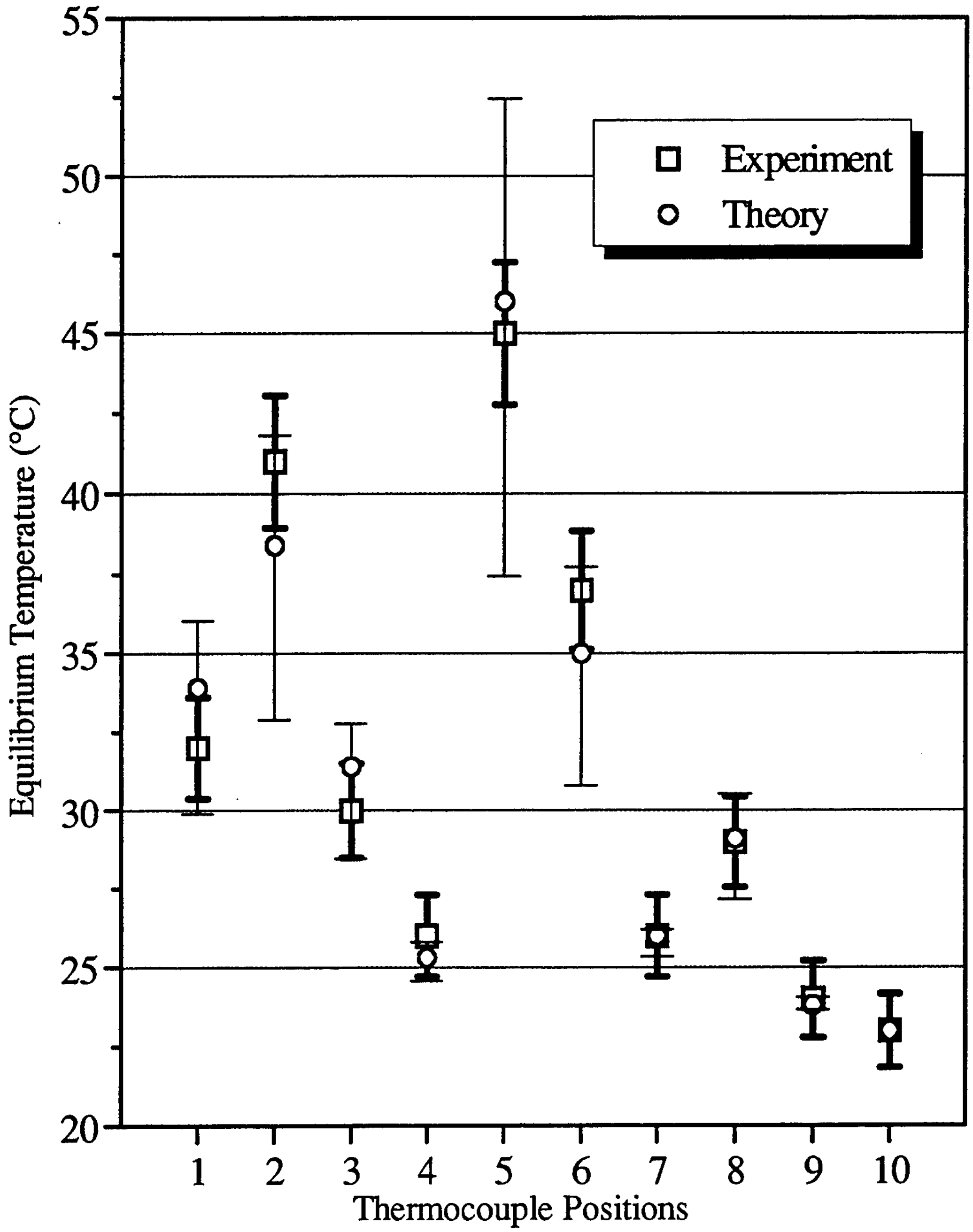

Figure 11. Experimental and Predicted Equilibrium Surface Temperature Data for Specimen (0_11_6) Including Appropriate Error for Each.

the heat-transfer analysis used in this study. Position No. 5 represents the point of highest heating in the specimen quadrant shown in Figure 12. The 1-D assumption may break down in light of the severe thermal gradients around thermocouple position No. 5. An analysis of the 3-D

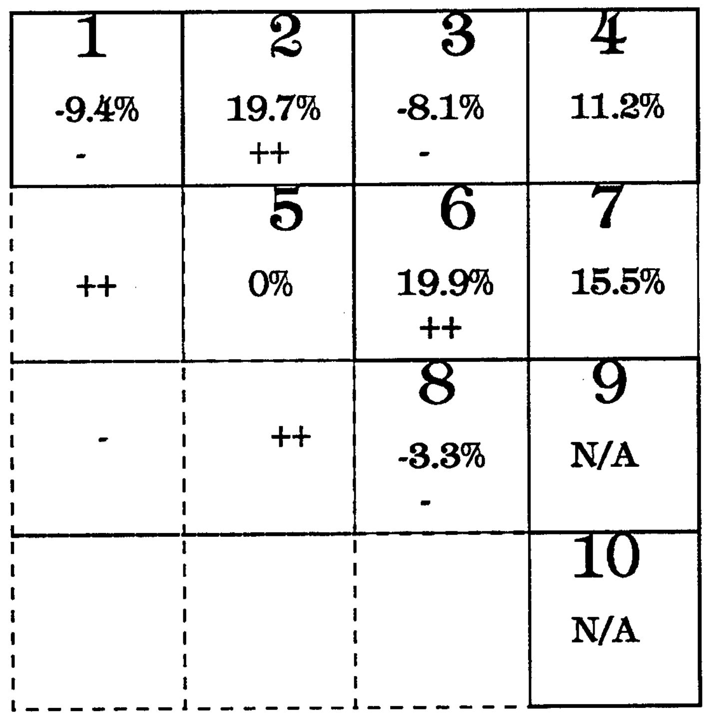

Figure 12. Diagram Showing Average Variation of Experimental Equilibrium Results From Predicted Equilibrium Results for All 10 Thermocouples.

heat-source distribution, provided by the in-plane planar grid and the through-thickness capacitive fiber layer models, which would provide a layer-by-layer anisotropic heat-transfer analysis would likely resolve these discrepancies. This is a topic of future work.

The positions of Nos. 2 and 6 in Figure 12 lie along fiber paths in the 0° and 90° plies; therefore, they are expected to heat somewhat faster than predicted due to the higher actual thermal conductivity in these directions vs. the effective properties used in our analysis. Likewise, the Nos. 1, 3, and 8 positions are expected to heat slower than predicted. The higher values in the Nos. 4 and 7 positions are not meaningful since the actual temperatures measured in these locations was very low. Position Nos. 9 and 10 were also low heating. Their percent-difference results are not included due to the insignificant temperature values recorded at these locations.

Again, tabular equilibrium results for all the 10-amp applied coil-current tests are available [2]. These tables, however, fail to indicate the transient behavior of the surface temperature, which would provide comparative information on heating rates. One way of providing this information is to represent transient behavior as a linear increase in temperature with time to an equilibrium temperature, T_{eq}, at time t_{eq}. The time to equilibrium is calculated from the transient results as the time to reach a temperature within 3% of the equilibrium temperature (taken at t = 180 s) as illustrated in Figure 13.

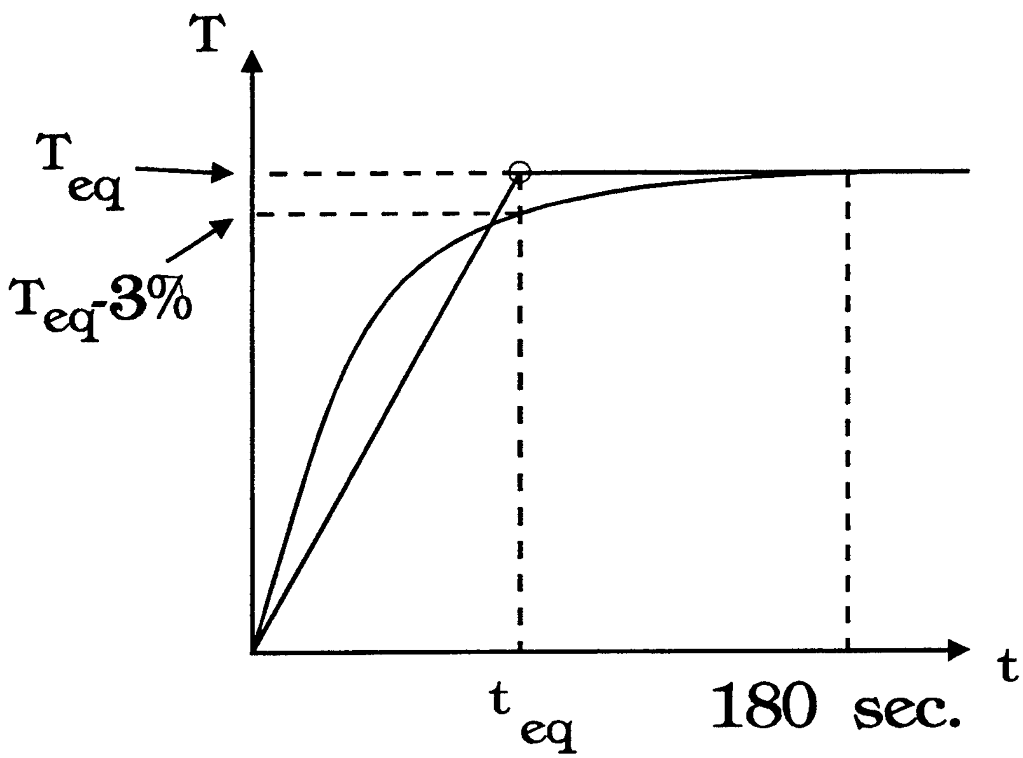

Figure 13. Schematic Definition of Equilibrium Temperature and Equilibrium Time. The Equilibrium Temperature Is Defined as the Temperature Measured at T = 180 s. The Equilibrium Time Is Defined as the Time at Which the Temperature Has Reached 3% of the Equilibrium Temperature. The "Time-Temperature Equilibrium Point" Is Marked With the Small Circle.

Although the various thermocouples (i.e., surface positions) reached equilibrium at different times, the average time to equilibrium is valuable for comparison between specimens. Figure 14 shows these calculated points in the thermal history data for the assumed linear heating profiles.

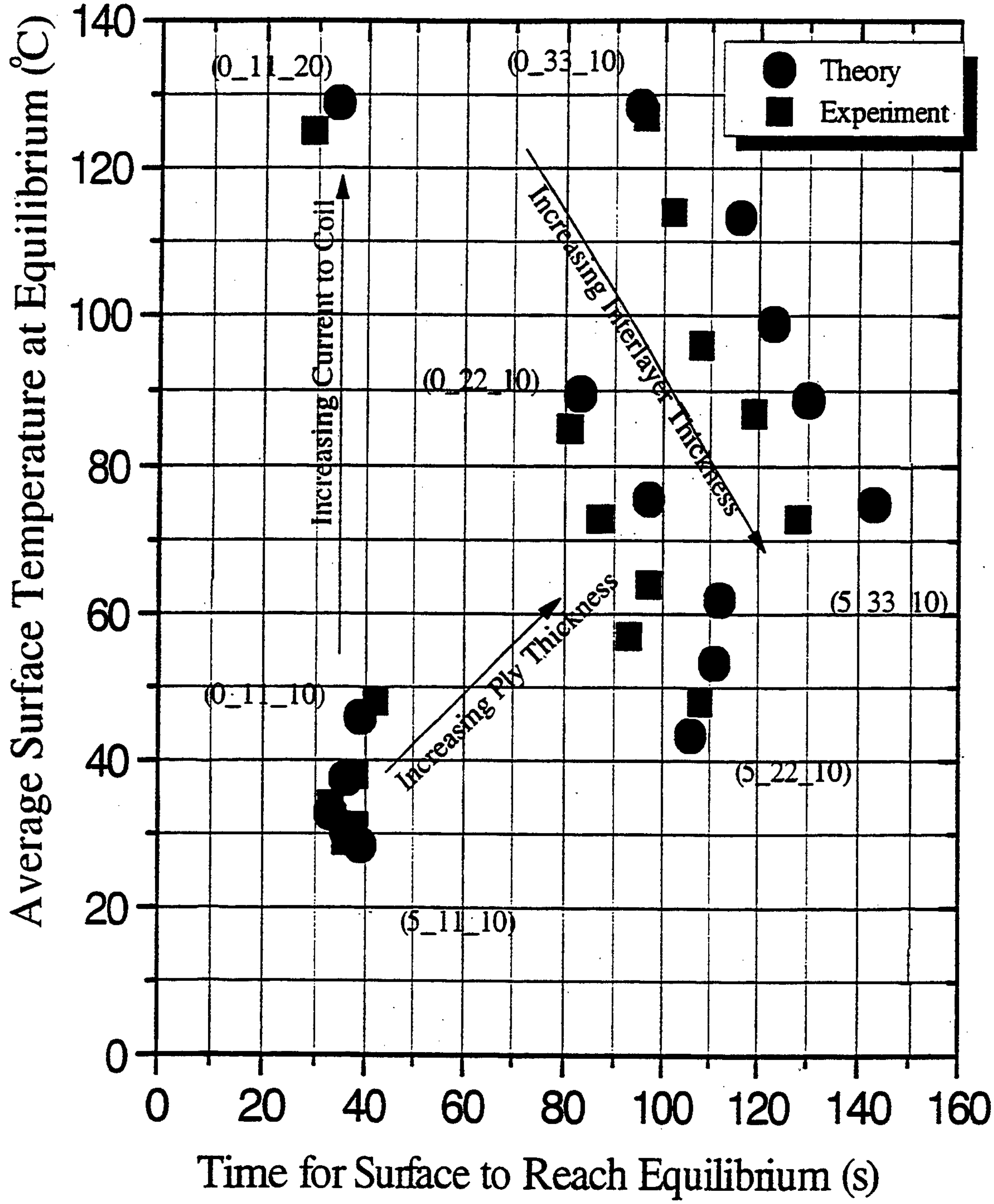

Figure 14. Summary of Time-Temperature Equilibrium Points.

Figure 14a shows that, as expected, T_{eq} and t_{eq} both increase with increasingly ply thickness; Teq increases due to the higher heating predicted by our theory, and t_{eq} increases due to the increased amount of material being heated. Figure 14b shows that increasing the interlayer thickness significantly decreases T_{eq} as predicted and slightly increases t_{eq} due to less significant increases in added material; however, the material that is added has a low thermal conductivity and is in the center of the specimen. Figure 14c shows that an increase in the current to the coil increases T_{eq} dramatically, yet the time to reach equilibrium does not change.

6.2 Effect of Varying Interface Thickness. The predicted effect of varying the interface thickness on the parameter γ (given in Figure 7) indicated a rapid decrease in the heating parameter γ with increasing interface resin thickness h_o. As noted previously, the point corresponding to the location of thermocouple No. 5 in Figure 4 represents the highest predicted and recorded heating in the plane. Figure 15 shows experimental data for the equilibrium (steady state) surface temperature at this point for the [0/90], $[0_2/90_2]$ and $[0_3/90_3]$ specimens at 10-amp current. The error bars on the experimental results are indicative of the ±1 °C reading of the digital thermocouple reader and an additional ±5% error on the accuracy of the placement of the thermocouple on the specimen. This value of 5% was determined by analyzing the changes in temperature over one square centimeter centered on the point of highest heating. Figure 16 compares predicted and experimental steady-state surface temperatures at this point for the [0/90] specimen [code (x_11_10)]. Experimental results agree quite well with predictions. Equivalent comparisons were obtained for other specimen/coil configurations [2].

6.3 Effect of Varying Ply Thickness. Figure 6 shows the predicted effect of increasing the ply thickness on the capacitive-layer-model's parameter γ. Moderate increases in the heating parameter γ were predicted for substantial increases in ply thickness. Figure 17 shows the observed effect of increasing the ply thickness on the equilibrium surface temperature at thermocouple No. 5 for various interply thicknesses. Although increasing ply thickness has little effect on the parameter γ, it has a more significant effect on the temperature. This is due to the significant increase in loss tangent of PEEK at the glass transition temperature, resulting in increased heating in those specimens that approach a temperature of 140 °C, as shown in Figure 6.

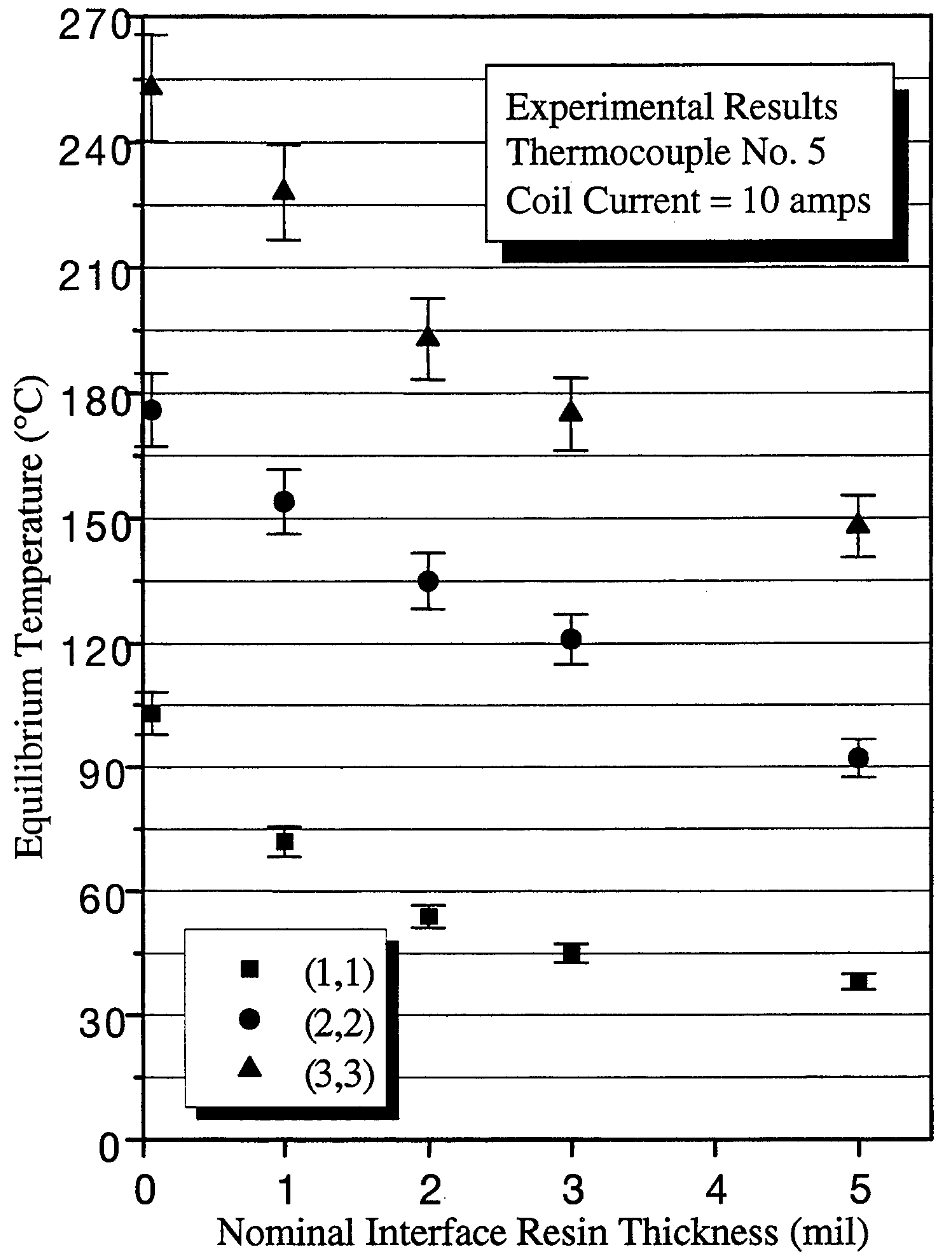

Figure 15. Experimental Results Showing Effect of Varying the Thickness of the Interfacial Resin Layer.

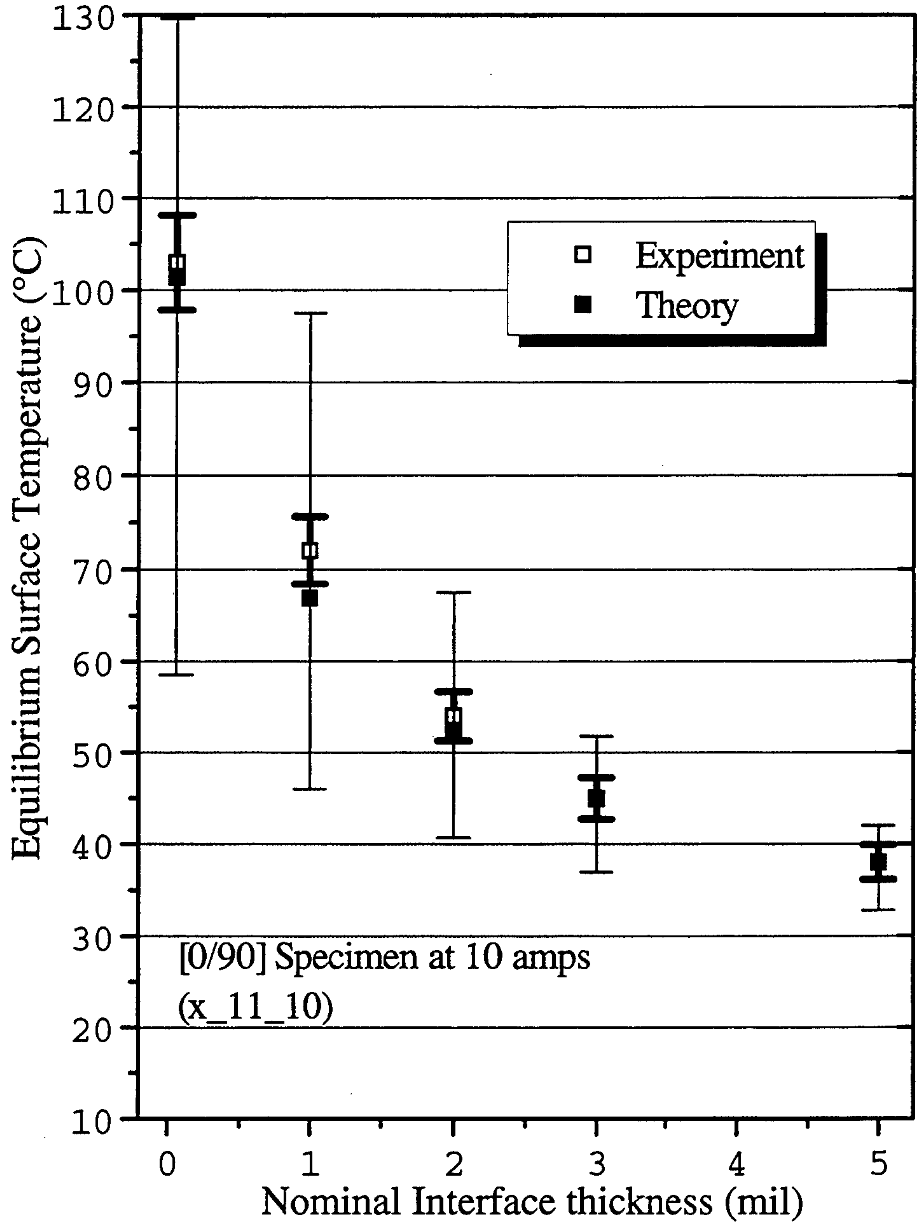

Figure 16. Comparison of Predicted and Observed Surface Temperatures Showing Effect of Increasing Interface Thickness, h_o, on Equilibrium Surface Temperature. The Heavy Lines Represent the Experimental Results, While the Thin Lines Represent Predicted Results With Upper and Lower Bounds.

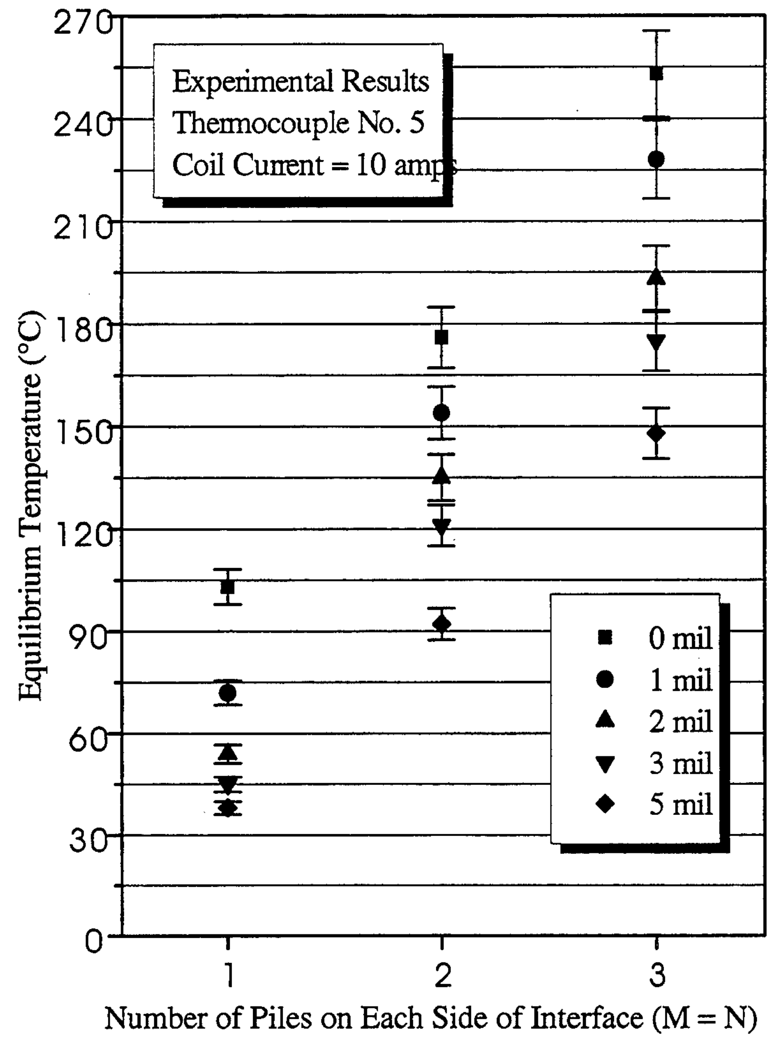

Figure 17. Experimental Observation Showing Effect of Increasing Ply Thickness on Equilibrium Surface Temperature for Various Interface Resin Thicknesses.

6.4 Effect of Varying Coil Current. Figure 18 shows the effect of varying the applied coil current (i.e., increasing the magnetic flux) on the (0_11_*I*) specimens using currents, *I*, of 6, 10 and 20 amp. A current-squared power relationship is expected. The curve fit shown on the graph is for the equation $T = 0.7(I)^2 + 23$ °C. With the loss tangent changing with temperature, the thermal data is expected to show a faster rise in temperature than for a constant loss tangent value. Therefore, the current-squared relationship includes both the resistive nature of heating and the variation of loss tangent with temperature, which is offset by the temperature-dependent convection and radiation losses.

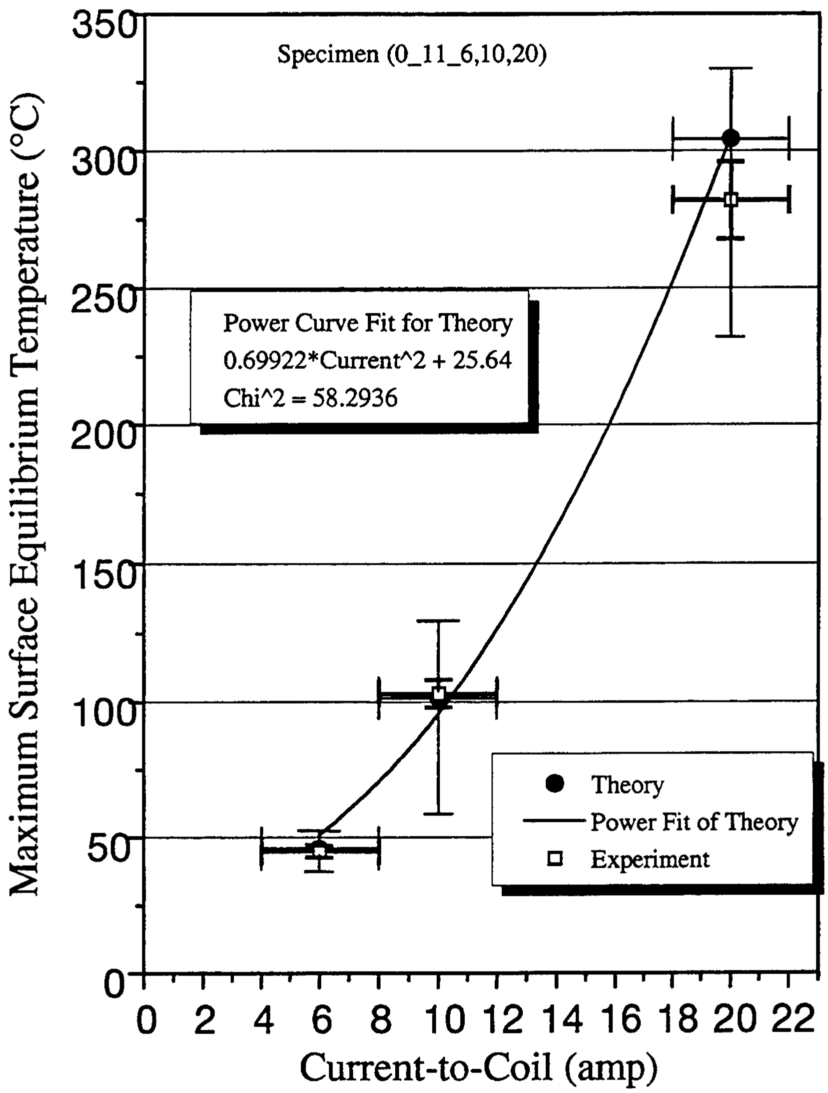

Figure 18. Comparison of Predicted and Observed Surface Temperatures Showing Effect of Applied Coil Current on Heating.

7. Summary

Local, in-plane, and through-thickness submodels were combined to provide input for a finite element heat-transfer analysis to predict transient thermal profile in the plane of thin laminates. Assumptions concerning through-thickness thermal gradients and linearity of potential field gradients in the plane were imposed to obtain a solution. The validity of the assumptions that encompass the thermal submodel are supported by the agreement with the model's output with experimental data. The convection heat-transfer coefficient was experimentally determined.

An experimental test matrix and apparatus were employed to verify the proposed theory of dielectric heating as the fundamental mechanism of thermal generation in continuous carbon-fiber thermoplastic-matrix cross-ply laminated composites subjected to a transverse magnetic field. It has been shown that, as the ply-ply interface resin-rich region thickness h_o increases, the heating in the laminate decreases significantly. This indicates that Joule heating due to fiber-fiber contact is not likely. Furthermore, increasing the number of plies on either side of the interface increases the heating indicating that thermal generation in the laminate is a function of ply thickness and most likely occurs throughout the thickness of the laminate.

The accuracy of the surface temperature measurements to those predicted under a variety of physical parameters gives credence to the validity of the original proposal stated in Fink, McCullough, and Gillespie [1]. Claims of Joule losses in the fibers [10–13], fiber contact resistance losses, and local-only heating at the ply-ply interface are not supported by the current experimental investigation. Joule losses in the fibers would result in constant heating on the perimeter of the Helmholtz-type coil—this was not the case; heating was shown to occur at precise points and with specific intensities as predicted by the global model. Fiber contact resistance losses, while potentially exhibiting similar qualitative heating patterns, would induce significant current in the fibers themselves, resulting in measurable Joule heating in the fibers. This was not witnessed in this study. Although not directly shown, the existence of the gradient of heating through the thickness of the laminate, as predicted by the capacitive fiber layer submodel, is indirectly supported by the model's ability to predict the total thermal generation. However, the quantitative summation of through-thickness heat generation was verified. If heating only occurred at the resin-rich ply-ply interface (h_o region), then the expected total heating would be significantly lower and result in significantly lower surface temperatures.

Continuing work involves extending the present theory and models to laminates containing off-axis plies and performing a 3-D heat-transfer analysis using anisotropic properties and a ply-by-ply approach. This will allow the investigation of thick laminates to further verify the through-thickness thermal generation model and provide insight into special problems associated with angle-ply laminates.

8. References

1. Fink, B. K., R. L. McCullough, and J. W. Gillespie, Jr. "A Local Theory of Heating in Cross-Ply Carbon Fiber Thermoplastic Composites by Magnetic Induction." *Polym. Eng. Sci.*, vol. 32, vol. 357, 1992.

2. Fink, B. K. Doctoral dissertation. University of Delaware, 1991.

3. Fink, B. K., R. L. McCullough, and J. W. Gillespie, Jr. "A Model to Predict the Planar Electrical Potential Distribution in Cross-Ply Carbon-Fiber Composites Subjected to Alternating Magnetic Fields." *Composites Science and Technology*, vol 49, no. 1, pp. 71–80, 1993.

4. Fink, B. K., R. L. McCullough, and J. W. Gillespie, Jr. "A Model to Predict the Through-Thickness Distribution of Heat Generation in Carbon-Fiber Composites Subjected to Alternating Magnetic Fields." *Composites Science and Technology*, vol. 55, pp. 119–130, 1995.

5. Fink, B. K., R. L. McCullough, and J. W. Gillespie, Jr. "The Influence of Moisture on Dielectric Behavior of Poly-Etheretherketone/Carbon Fiber Composites." *Journal of Thermoplastic Composite Materials*, vol. 5, pp. 90–104, 1992.

6. ICI Advanced Materials. "Victrex PEEK 450G." 1985.

7. Jakobsen, T. B., R. C. Don, and J. W. Gillespie, Jr. *Polym. Eng. Sci.* Vol. 29, p. 1722, 1989.

8. Hercules Inc. "Magnamite Graphite Fiber Type AS4." 1990.

9. ICI Fiberite. "Property Data of Aromatic Polymer Composite: APC-2/Hercules Magnamite AS-4 Carbon Fiber." 1986.

10. Border, J., and R. Salas. "Induction Heated Joining of Thermoplastic Composites Without Metal Susceptors." 34th SAMPE Symp. Proc., 1989.

11. Border, J. "Understanding Induction Heating and Its Utilization for Aircraft Structural Repair." PDA-89-FR-5865-00-2, PDA Engineering, 1989.

12. Miller, A. K., C. Chang, A. Payne, M. Gur, E. Menzel, and A. Peled. *SAMPE J.* Vol. 26, no. 4, p. 37, 1990.

13. Xiao, X. R., S. V. Hoa, and K. N. Street. "Repair of Thermoplastic Composite Structures by Fusion Bonding." SAMPE Symp. Proc., 1990.

INTENTIONALLY LEFT BLANK.

NO. OF COPIES	ORGANIZATION
2	DEFENSE TECHNICAL INFORMATION CENTER DTIC DDA 8725 JOHN J KINGMAN RD STE 0944 FT BELVOIR VA 22060-6218
1	HQDA DAMO FDT 400 ARMY PENTAGON WASHINGTON DC 20310-0460
1	OSD OUSD(A&T)/ODDDR&E(R) R J TREW THE PENTAGON WASHINGTON DC 20301-7100
1	DPTY CG FOR RDA US ARMY MATERIEL CMD AMCRDA 5001 EISENHOWER AVE ALEXANDRIA VA 22333-0001
1	INST FOR ADVNCD TCHNLGY THE UNIV OF TEXAS AT AUSTIN PO BOX 202797 AUSTIN TX 78720-2797
1	DARPA B KASPAR 3701 N FAIRFAX DR ARLINGTON VA 22203-1714
1	NAVAL SURFACE WARFARE CTR CODE B07 J PENNELLA 17320 DAHLGREN RD BLDG 1470 RM 1101 DAHLGREN VA 22448-5100
1	US MILITARY ACADEMY MATH SCI CTR OF EXCELLENCE DEPT OF MATHEMATICAL SCI MADN MATH THAYER HALL WEST POINT NY 10996-1786

NO. OF COPIES	ORGANIZATION
1	DIRECTOR US ARMY RESEARCH LAB AMSRL D D R SMITH 2800 POWDER MILL RD ADELPHI MD 20783-1197
1	DIRECTOR US ARMY RESEARCH LAB AMSRL DD 2800 POWDER MILL RD ADELPHI MD 20783-1197
1	DIRECTOR US ARMY RESEARCH LAB AMSRL CS AS (RECORDS MGMT) 2800 POWDER MILL RD ADELPHI MD 20783-1145
3	DIRECTOR US ARMY RESEARCH LAB AMSRL CI LL 2800 POWDER MILL RD ADELPHI MD 20783-1145

ABERDEEN PROVING GROUND

NO. OF COPIES	ORGANIZATION
4	DIR USARL AMSRL CI LP (BLDG 305)

NO. OF COPIES	ORGANIZATION
1	DIRECTOR US ARMY RESEARCH LAB AMSRL CP CA D SNIDER 2800 POWDER MILL RD ADELPHI MD 20783-1145
1	DIRECTOR US ARMY RESEARCH LAB AMSRL OP SD TA 2800 POWDER MILL ROAD ADELPHI MD 20783-1145
3	DIRECTOR US ARMY RESEARCH LAB AMSRL OP SD TL 2800 POWDER MILL ROAD ADELPHI MD 20783-1145
1	DIRECTOR US ARMY RESEARCH LAB AMSRL OP SD TP 2800 POWDER MILL ROAD ADELPHI MD 20783-1145
2	DIRECTOR US ARMY RESEARCH LAB AMSRL OP CI AD TECH PUB BR RECORDS MGMT ADMIN 2800 POWDER MILL ROAD ADELPHI MD 20783-1197
1	HQDA DAMI FIT NOLAN BLDG WASHINGTON DC 20310-1025
1	DIRECTOR DA OASARDA SARD SO 103 ARMY PENTAGON WASHINGTON DC 20310-0103
1	DEPUTY ASST SCY FOR R&T SARD TT RM 3EA79 THE PENTAGON WASHINGTON DC 20301-7100

NO. OF COPIES	ORGANIZATION
1	COMMANDER US ARMY MATERIEL CMD AMXMI INT 5001 EISENHOWER AVE ALEXANDRIA VA 22333-0001
2	COMMANDER US ARMY ARDEC AMSTA AR AE WW E BAKER J PEARSON PICATINNY ARSENAL NJ 07806-5000
1	COMMANDER US ARMY ARDEC AMSTA AR TD C SPINELLI PICATINNY ARSENAL NJ 07806-5000
1	COMMANDER US ARMY ARDEC AMSTA AR FSE T GORA PICATINNY ARSENAL NJ
6	COMMANDER US ARMY ARDEC AMSTA AR CCH A W ANDREWS S MUSALLI R CARR M LUCIANO E LOGSDEN T LOUZEIRO PICATINNY ARSENAL NJ 07806-5000
4	COMMANDER US ARMY ARDEC AMSTA AR CC G PAYNE J GEHBAUER C BAULIEU H OPAT PICATINNY ARSENAL NJ 07806-5000

NO. OF COPIES	ORGANIZATION
1	COMMANDER US ARMY ARDEC AMSTA AR CCH P J LUTZ PICATINNY ARSENAL NJ 07806-5000
1	COMMANDER US ARMY ARDEC AMSTA AR FSF T C LIVECCHIA PICATINNY ARSENAL NJ 07806-5000
1	COMMANDER US ARMY ARDEC AMSTA AR QAC T C C PATEL PICATINNY ARSENAL NJ 07806-5000
2	COMMANDER US ARMY ARDEC AMSTA AR M D DEMELLA F DIORIO PICATINNY ARSENAL NJ 07806-5000
3	COMMANDER US ARMY ARDEC AMSTA AR FSA A WARNASH B MACHAK M CHIEFA PICATINNY ARSENAL NJ 07806-5000
2	COMMANDER US ARMY ARDEC AMSTA AR FSP G M SCHIKSNIS D CARLUCCI PICATINNY ARSENAL NJ 07806-5000

NO. OF COPIES	ORGANIZATION
1	COMMANDER US ARMY ARDEC AMSTA AR FSP A P KISATSKY PICATINNY ARSENAL NJ 07806-5000
2	COMMANDER US ARMY ARDEC AMSTA AR CCH C H CHANIN S CHICO PICATINNY ARSENAL NJ 07806-5000
9	COMMANDER US ARMY ARDEC AMSTA AR CCH B P DONADIA F DONLON P VALENTI C KNUTSON G EUSTICE S PATEL G WAGNECZ R SAYER F CHANG PICATINNY ARSENAL NJ 07806-5000
6	COMMANDER US ARMY ARDEC AMSTA AR CCL F PUZYCKI R MCHUGH D CONWAY E JAROSZEWSKI R SCHLENNER M CLUNE PICATINNY ARSENAL NJ 07806-5000
1	COMMANDER US ARMY ARDEC AMSTA AR QAC T D RIGOGLIOSO PICATINNY ARSENAL NJ 07806-5000

NO. OF COPIES	ORGANIZATION
1	COMMANDER US ARMY ARDEC AMSTA AR SRE D YEE PICATINNY ARSENAL NJ 07806-5000
1	COMMANDER US ARMY ARDEC AMSTA AR WET T SACHAR BLDG 172 PICATINNY ARSENAL NJ 07806-5000
1	COMMANDER US ARMY ARDEC SMCAR ASF PICATINNY ARSENAL NJ 07806-5000
1	COMMANDER US ARMY ARDEC AMSTA AR WEL F INTELLIGENCE SPECIALIST M GUERRIERE PICATINNY ARSENAL NJ 07806-5000
11	PROJECT MANAGER TANK MAIN ARMAMENT SYSTEMS SFAE GSSC TMA R MORRIS C KIMKER D GUZOWICZ E KOPACZ R ROESER R DARCY R MCDANOLDS L D ULISSE C ROLLER J MCGREEN B PATTER PICATINNY ARSENAL NJ 07806-5000

NO. OF COPIES	ORGANIZATION
2	PEO FIELD ARTILLERY SYSTEMS SFAE FAS PM H GOLDMAN T MCWILLIAMS PICATINNY ARSENAL NJ 07806-5000
6	PM SADARM SFAE GCSS SD COL B ELLIS M DEVINE R KOWALSKI W DEMASSI J PRITCHARD S HROWNAK PICATINNY ARSENAL NJ 07806-5000
1	COMMANDER US ARMY ARDEC PRODUCTION BASE MODERN ACTY AMSMC PBM K PICATINNY ARSENAL NJ 07806-5000
3	COMMANDER U S ARMY TACOM PM TACTICAL VEHICLES SFAE TVL SFAE TVM SFAE TVH 6501 ELEVEN MILE RD WARREN MI 48397-5000
1	COMMANDER U S ARMY TACOM PM ABRAMS SFAE ASM AB 6501 ELEVEN MILE RD WARREN MI 48397-5000
1	COMMANDER U S ARMY TACOM PM BFVS SFAE ASM BV 6501 ELEVEN MILE RD WARREN MI 48397-5000

NO. OF COPIES	ORGANIZATION
1	COMMANDER U S ARMY TACOM PM AFAS SFAE ASM AF 6501 ELEVEN MILE RD WARREN MI 48397-5000
2	COMMANDER U S ARMY TACOM PM SURV SYS SFAE ASM SS T DEAN SFAE GCSS W GSI M D COCHRAN 6501 ELEVEN MILE RD WARREN MI 48397-5000
1	COMMANDER U S ARMY TACOM PM RDT&E SFAE GCSS W AB J GODELL 6501 ELEVEN MILE RD WARREN MI 48397-5000
1	COMMANDER U S ARMY TACOM PM SURVIVABLE SYSTEMS SFAE GCSS W GSI H M RYZYI 6501 ELEVEN MILE RD WARREN MI 48397-5000
1	COMMANDER U S ARMY TACOM PM BFV SFAE GCSS W BV S DAVIS 6501 ELEVEN MILE RD WARREN MI 48397-5000
1	COMMANDER U S ARMY TACOM PM LIGHT TACTICAL VEHICLES AMSTA TR S AJ J MILLS MS 209 6501 ELEVEN MILE RD WARREN MI 48397-5000

NO. OF COPIES	ORGANIZATION
1	COMMANDER U S ARMY TACOM PM GROUND SYSTEMS INTEGRATION SFAE GCSS W GSI R LABATILLE 6501 ELEVEN MILE RD WARREN MI 48397-5000
1	COMMANDER U S ARMY TACOM CHIEF ABRAMS TESTING SFAE GCSS W AB QT T KRASKIEWICZ 6501 ELEVEN MILE RD WARREN MI 48397-5000
1	COMMANDER US ARMY TACOM AMSTA SF WARREN MI 48397-5000
1	COMMANDER SMCWV QAE Q B VANINA BLDG 44 WATERVLIET ARSENAL WATERVLIET NY 12189-4050
14	COMMANDER US ARMY TACOM ASMTA TR R J CHAPIN R MCCLELLAND D THOMAS J BENNETT D HANSEN AMSTA JSK S GOODMAN J FLORENCE K IYER J THOMSON AMSTA TR D D OSTBERG L HINOJOSA B RAJU AMSTA CS SF H HUTCHINSON F SCHWARZ WARREN MI 48397-5000

NO. OF COPIES	ORGANIZATION
1	COMMANDER SMCWV SPM T MCCLOSKEY BLDG 253 WATERVLIET ARSENAL WATERVLIET NY 12189-4050
10	BENET LABORATORIES AMSTA AR CCB R FISCELLA G D ANDREA M SCAVULO G SPENCER P WHEELER K MINER J VASILAKIS G FRIAR R HASENBEIN SMCAR CCB R S SOPOK WATERVLIET NY 12189
2	TSM ABRAMS ATZK TS S JABURG W MEINSHAUSEN FT KNOX KY 40121
3	ARMOR SCHOOL ATTN ATZK TD R BAUEN J BERG A POMEY FT KNOX KY 40121
2	HQ IOC TANK AMMO TEAM AMSIO SMT R CRAWFORD W HARRIS ROCK ISLAND IL 61299-6000
1	DIRECTOR U S ARMY AMCOM SFAE AV RAM TV D CALDWELL BUILDING 5300 REDSTONE ARSENAL AL 35898

NO. OF COPIES	ORGANIZATION
4	DIRECTOR US ARMY CECOM NIGHT VISION AND ELECTRONIC SENSORS DIRECTORATE AMSEL RD NV CM CCD R ADAMS R MCLEAN A YINGST AMSEL RD NV VISP E JACOBS 10221 BURBECK RD FT BELVOIR VA 22060-5806
2	CDR USA AMCOM AVIATION APPLIED TECH DIR J SCHUCK FT EUSTIS VA 23604-5577
1	U S ARMY CRREL P DUTTA 72 LYME RD HANOVER NH 03755
1	US ARMY CERL R LAMPO 2902 NEWMARK DR CHAMPAIGN IL 61822
2	U S ARMY CORP OF ENGINEERS CERD C T LIU CEW ET T TAN 20 MASS AVE NW WASHINGTON DC 20314
10	DIRECTOR US ARMY NATL GRND INTEL CTR D LEITER S EITELMAN M HOLTUS M WOLFE S MINGLEDORF H C ARDLEIGH J GASTON W GSTATTENBAUER R WARNER J CRIDER 220 SEVENTH STREET NE CHARLOTTESVILLE VA 22091

NO. OF COPIES	ORGANIZATION
6	US ARMY SBCCOM SOLDIER SYSTEMS CENTER BALLISTICS TEAM J WARD MARINE CORPS TEAM J MACKIEWICZ BUS AREA ADVOCACY TEAM W HASKELL SSCNC WST W NYKVIST T MERRILL S BEAUDOIN KANSAS ST NATICK MA 01760-5019
1	US ARMY COLD REGIONS RSCH & ENGRNG LAB P DUTTA 72 LYME RD HANOVER NH 03755
1	SYSTEM MANAGER ABRAMS BLDG 1002 RM 110 ATZK TS LTC J H NUNN FT KNOX KY 40121
9	US ARMY RESEARCH OFFICE A CROWSON J CHANDRA H EVERETT J PRATER R SINGLETON G ANDERSON D STEPP D KISEROW J CHANG PO BOX 12211 RESEARCH TRIANGLE PARK NC 27709-2211
1	DIRECTORATE OF CMBT DEVELOPMENT C KJORO 320 ENGINEER LOOP STE 141 FT LEONARD WOOD MO 65473-8929

NO. OF COPIES	ORGANIZATION
1	COMMANDANT U S ARMY FIELD ARTILLERY CTR AT FT SILL ATFS CD LTC BUMGARNER FT SILL OK 73503 5600
1	CHIEF USAIC LTC T J CUMMINGS ATZB COM FT BENNING GA 31905-5800
1	NAVAL AIR SYSTEMS CMD J THOMPSON 48142 SHAW RD UNIT 5 PATUXENT RIVER MD 20670
1	NAVAL SURFACE WARFARE CTR DAHLGREN DIV CODE G06 DAHLGREN VA 22448
1	NAVAL SURFACE WARFARE CTR TECH LIBRARY CODE 323 17320 DAHLGREN RD DAHLGREN VA 22448
3	NAVAL RESEARCH LAB I WOLOCK CODE 6383 R BADALIANCE CODE 6304 L GAUSE WASHINGTON DC 20375
1	NAVAL SURFACE WARFARE CTR CRANE DIVISION M JOHNSON CODE 20H4 LOUISVILLE KY 40214-5245
2	COMMANDER NAVAL SURFACE WARFARE CTR CADEROCK DIVISION R PETERSON CODE 2020 M CRITCHFIELD CODE 1730 BETHESDA MD 20084
2	NAVAL SURFACE WARFARE CTR U SORATHIA C WILLIAMS CD 6551 9500 MACARTHUR BLVD WEST BETHESDA MD 20817

NO. OF COPIES	ORGANIZATION
1	DAVID TAYLOR RESEARCH CTR SHIP STRUCTURES & PROTECTION DEPARTMENT CODE 1702 J CORRADO BETHESDA MD 20084
2	DAVID TAYLOR RESEARCH CTR R ROCKWELL W PHYILLAIER BETHESDA MD 20054-5000
1	OFFICE OF NAVAL RESEARCH D SIEGEL CODE 351 800 N QUINCY ST ARLINGTON VA 22217-5660
8	NAVAL SURFACE WARFARE CTR J FRANCIS CODE G30 D WILSON CODE G32 R D COOPER CODE G32 J FRAYSSE CODE G33 E ROWE CODE G33 T DURAN CODE G33 L DE SIMONE CODE G33 R HUBBARD CODE G33 DAHLGREN VA 22448
1	NAVAL SEA SYSTEMS CMD D LIESE 2531 JEFFERSON DAVIS HIGHWAY ARLINGTON VA 22242-5160
1	NAVAL SURFACE WARFARE M LACY CODE B02 17320 DAHLGREN RD DAHLGREN VA 22448
1	OFFICE OF NAVAL RES J KELLY 800 NORTH QUINCEY ST ARLINGTON VA 22217-5000
2	NAVAL SURFACE WARFARE CTR CARDEROCK DIVISION R CRANE CODE 2802 C WILLIAMS CODE 6553 3A LEGGETT CIR BETHESDA MD 20054-5000

NO. OF COPIES	ORGANIZATION
1	NAVSEA OJRI PEO DD21 PMS500 G CAMPONESCHI 2351 JEFFERSON DAVIS HWY ARLINGTON VA 22242-5165
1	EXPEDITIONARY WARFARE DIV N85 F SHOUP 2000 NAVY PENTAGON WASHINGTON DC 20350-2000
1	AFRL MLBC 2941 P STREET RM 136 WRIGHT PATTERSON AFB OH 45433-7750
1	AFRL MLSS R THOMSON 2179 12TH STREET RM 122 WRIGHT PATTERSON AFB OH 45433-7718
2	AFRL F ABRAMS J BROWN BLDG 653 2977 P STREET STE 6 WRIGHT PATTERSON AFB OH 45433-7739
1	AFRL MLS OL 7278 4TH STREET BLDG 100 BAY D L COULTER HILL AFB UT 84056-5205
1	OSD JOINT CCD TEST FORCE OSD JCCD R WILLIAMS 3909 HALLS FERRY RD VICKSBURG MS 29180-6199
1	DEFENSE NUCLEAR AGENCY INNOVATIVE CONCEPTS DIV R ROHR 6801 TELEGRAPH RD ALEXANDRIA VA 22310-3398

NO. OF COPIES	ORGANIZATION
1	WATERWAYS EXPERIMENT D SCOTT 3909 HALLS FERRY RD SC C VICKSBURG MS 39180
3	DARPA M VANFOSSEN S WAX L CHRISTODOULOU 3701 N FAIRFAX DR ARLINGTON VA 22203-1714
2	SERDP PROGRAM OFC PM P2 C PELLERIN B SMITH 901 N STUART ST SUITE 303 ARLINGTON VA 22203
1	FAA MIL HDBK 17 CHAIR L ILCEWICZ 1601 LIND AVE SW ANM 115N RENTON VA 98055
2	FAA TECH CENTER D OPLINGER AAR 431 P SHYPRYKEVICH AAR 431 ATLANTIC CITY NJ 08405
1	OFC OF ENVIRONMENTAL MGMT U S DEPT OF ENERGY P RITZCOVAN 19901 GERMANTOWN RD GERMANTOWN MD 20874-1928
1	LOS ALAMOS NATL LAB F ADDESSIO MS B216 PO BOX 1633 LOS ALAMOS NM 87545
1	OAK RIDGE NATL LAB R M DAVIS PO BOX 2008 OAK RIDGE TN 37831-6195

NO. OF COPIES	ORGANIZATION
5	DIRECTOR LAWRENCE LIVERMORE NATL LAB R CHRISTENSEN S DETERESA F MAGNESS M FINGER MS 313 M MURPHY L 282 PO BOX 808 LIVERMORE CA 94550
7	NIST R PARNAS J DUNKERS M VANLANDINGHAM MS 8621 J CHIN MS 8621 D HUNSTON MS 8543 J MARTIN MS 8621 D DUTHINH MS 8611 100 BUREAU DR GAITHERSBURG MD 20899
1	OAK RIDGE NATL LAB C EBERLE MS 8048 PO BOX 2009 OAK RIDGE TN 37831
1	OAK RIDGE NATL LAB C D WARREN MS 8039 PO BOX 2009 OAK RIDGE TN 37922
4	DIRECTOR SANDIA NATL LABS APPLIED MECHANICS DEPT DIVISION 8241 W KAWAHARA K PERANO D DAWSON P NIELAN PO BOX 969 LIVERMORE CA 94550-0096
1	LAWRENCE LIVERMORE NATIONAL LAB M MURPHY PO BOX 808 L 282 LIVERMORE CA 94550

NO. OF COPIES	ORGANIZATION
3	NASA LANGLEY RESEARCH CTR MS 266 AMSRL VS W ELBER F BARTLETT JR G FARLEY HAMPTON VA 23681-0001
1	NASA LANGLEY RESEARCH CTR T GATES MS 188E HAMPTON VA 23661-3400
1	USDOT FEDERAL RAILROAD RDV 31 M FATEH WASHINGTON DC 20590
1	DOT FHWA J SCALZI 400 SEVENTH ST SW 3203 HNG 32 WASHINGTON DC 20590
1	FHWA E MUNLEY 6300 GEORGETOWN PIKE MCLEAN VA 22101
1	CENTRAL INTELLIGENCE AGENCY OTI WDAG GT W L WALTMAN PO BOX 1925 WASHINGTON DC 20505
1	MARINE CORPS INTEL ACTY D KOSITZKE 3300 RUSSELL RD SUITE 250 QUANTICO VA 22134-5011
1	NATL GRND INTELLIGENCE CTR DIRECTOR IANG TMT 220 SEVENTH ST NE CHARLOTTESVILLE VA 22902-5396
1	DIRECTOR DEFENSE INTELLIGENCE AGENCY TA 5 K CRELLING WASHINGTON DC 20310

NO. OF COPIES	ORGANIZATION
1	GRAPHITE MASTERS INC J WILLIS 3815 MEDFORD ST LOS ANGELES CA 90063-1900
1	ADVANCED GLASS FIBER YARNS T COLLINS 281 SPRING RUN LN STE A DOWNINGTON PA 19335
1	COMPOSITE MATERIALS INC D SHORTT 19105 63 AVE NE PO BOX 25 ARLINGTON WA 98223
1	COMPOSITE MATERIALS INC R HOLLAND 11 JEWEL COURT ORINDA CA 94563
1	COMPOSITE MATERIALS INC C RILEY 14530 S ANSON AVE SANTA FE SPRINGS CA 90670
2	COMPOSIX D BLAKE L DIXON 120 O NEILL DR HEBRUN OHIO 43025
4	CYTEC FIBERITE R DUNNE D KOHLI M GILLIO R MAYHEW 1300 REVOLUTION ST HAVRE DE GRACE MD 21078
2	SIMULA J COLTMAN R HUYETT 10016 S 51ST ST PHOENIX AZ 85044
1	SIOUX MFG B KRIEL PO BOX 400 FT TOTTEN ND 58335

NO. OF COPIES	ORGANIZATION
2	PROTECTION MATERIALS INC M MILLER F CRILLEY 14000 NW 58 CT MIAMI LAKES FL 33014
3	FOSTER MILLER J J GASSNER M ROYLANCE W ZUKAS 195 BEAR HILL RD WALTHAM MA 02354-1196
1	ROM DEVELOPMENT CORP R O MEARA 136 SWINEBURNE ROW BRICK MARKET PLACE NEWPORT RI 02840
2	TEXTRON SYSTEMS T FOLTZ M TREASURE 201 LOWELL ST WILMINGTON MA 08870-2941
1	JPS GLASS L CARTER PO BOX 260 SLATER RD SLATER SC 29683
1	O GARA HESS & EISENHARDT M GILLESPIE 9113 LESAINT DR FAIRFIELD OH 45014
2	MILLIKEN RESEARCH CORP H KUHN M MACLEOD PO BOX 1926 SPARTANBURG SC 29303
1	CONNEAUGHT INDUSTRIES INC J SANTOS PO BOX 1425 COVENTRY RI 02816

NO. OF COPIES	ORGANIZATION
1	BATTELLE C R HARGREAVES 505 KING AVE COLUMBUS OH 43201-2681
2	BATTELLE NATICK OPERATIONS J CONNORS B HALPIN 209 W CENTRAL ST STE 302 NATICK MA 01760
1	BATTELLE NW DOE PNNL T HALL MS K231 BATTELLE BLVD RICHLAND WA 99352
3	PACIFIC NORTHWEST LAB M SMITH G VAN ARSDALE R SHIPPELL PO BOX 999 RICHLAND WA 99352
1	ARMTEC DEFENSE PRODUCTS S DYER 85 901 AVE 53 PO BOX 848 COACHELLA CA 92236
2	ADVANCED COMPOSITE MATLS CORP P HOOD J RHODES 1525 S BUNCOMBE RD GREER SC 29651-9208
2	GLCC INC J RAY M BRADLEY 103 TRADE ZONE DR STE 26C WEST COLUMBIA SC 29170
2	AMOCO PERFORMANCE PRODUCTS M MICHNO JR J BANISAUKAS 4500 MCGINNIS FERRY RD ALPHARETTA GA 30202-3944

NO. OF COPIES	ORGANIZATION
1	SAIC M PALMER 2109 AIR PARK RD S E ALBUQUERQUE NM 87106
1	SAIC ATTN G CHRYSSOMALLIS 3800 W 80TH ST STE 1090 BLOOMINGTON MN 55431
1	AAI CORPORATION DR T G STASTNY PO BOX 126 HUNT VALLEY MD 21030-0126
1	JOHN HEBERT PO BOX 1072 HUNT VALLEY MD 21030-0126
12	ALLIANT TECHSYSTEMS INC C CANDLAND C AAKHUS R BECKER B SEE N VLAHAKUS R DOHRN S HAGLUND D FISHER W WORRELL R COPENHAFER M HISSONG D KAMDAR 600 2ND ST NE HOPKINS MN 55343-8367
3	ALLIANT TECHSYSTEMS INC J CONDON E LYNAM J GERHARD WV01 16 STATE RT 956 PO BOX 210 ROCKET CENTER WV 26726-0210
1	APPLIED COMPOSITES W GRISCH 333 NORTH SIXTH ST ST CHARLES IL 60174

NO. OF COPIES	ORGANIZATION
1	PROJECTILE TECHNOLOGY INC 515 GILES ST HAVRE DE GRACE MD 21078
1	CUSTOM ANALYTICAL ENG SYS INC A ALEXANDER 13000 TENSOR LN NE FLINTSTONE MD 21530
2	LORAL VOUGHT SYSTEMS G JACKSON K COOK 1701 W MARSHALL DR GRAND PRAIRIE TX 75051
5	AEROJET GEN CORP D PILLASCH T COULTER C FLYNN D RUBAREZUL M GREINER 1100 WEST HOLLYVALE ST AZUSA CA 91702-0296
3	HEXCEL INC R BOE F POLICELLI J POESCH PO BOX 98 MAGNA UT 84044
3	HERCULES INC G KUEBELER J VERMEYCHUK B MANDERVILLE JR HERCULES PLAZA WILMINGTON DE 19894
1	BRIGS COMPANY J BACKOFEN 2668 PETERBOROUGH ST HERDON VA 22071-2443
1	ZERNOW TECHNICAL SERVICES L ZERNOW 425 W BONITA AVE STE 208 SAN DIMAS CA 91773

NO. OF COPIES	ORGANIZATION
2	OLIN CORPORATION FLINCHBAUGH DIV E STEINER B STEWART PO BOX 127 RED LION PA 17356
1	OLIN CORPORATION L WHITMORE 10101 9TH ST NORTH ST PETERSBURG FL 33702
1	DOW UT S TIDRICK 15 STERLING DR WALLINGFORD CT 06492
5	SIKORSKY AIRCRAFT G JACARUSO T CARSTENSAN B KAY S GARBO M S S330A J ADELMANN 6900 MAIN ST PO BOX 9729 STRATFORD CT 06497-9729
1	PRATT & WHITNEY D HAMBRICK 400 MAIN ST MS 114 37 EAST HARTFORD CT 06108
1	AEROSPACE CORP G HAWKINS M4 945 2350 E EL SEGUNDO BLVD EL SEGUNDO CA 90245
2	CYTEC FIBERITE M LIN W WEB 1440 N KRAEMER BLVD ANAHEIM CA 92806
1	HEXCEL T BITZER 11711 DUBLIN BLVD DUBLIN CA 94568

NO. OF COPIES	ORGANIZATION
1	BOEING R BOHLMANN PO BOX 516 MC 5021322 ST LOUIS MO 63166-0516
2	BOEING DEFENSE AND SPACE GRP W HAMMOND J RUSSELL S 4X55 PO BOX 3707 SEATTLE WA 98124-2207
2	BOEING ROTORCRAFT P MINGURT P HANDEL 800 B PUTNAM BLVD WALLINGFORD PA 19086
1	BOEING DOUGLAS PRODUCTS DIV L J HART SMITH 3855 LAKEWOOD BLVD D800 0019 LONG BEACH CA 90846-0001
1	LOCKHEED MARTIN S REEVE 8650 COBB DR D 73 62 MZ 0648 MARIETTA GA 30063-0648
1	LOCKHEED MARTIN SKUNK WORKS D FORTNEY 1011 LOCKHEED WAY PALMDALE CA 93599-2502
1	LOCKHEED MARTIN R FIELDS 1195 IRWIN CT WINTER SPRINGS FL 32708
1	MATERIALS SCIENCES CORP B W ROSEN 500 OFFICE CENTER DR STE 250 FORT WASHINGTON PA 19034

NO. OF COPIES	ORGANIZATION
1	NORTHRUP GRUMMAN CORP ELECTRONIC SENSORS & SYSTEMS DIV E SCHOCH 1745A WEST NURSERY RD MAILSTOP V 16 LINTHICUM MD 21090
2	NORTHROP GRUMMAN ENVIRONMENTAL PROGRAMS R OSTERMAN A YEN 8900 E WASHINGTON BLVD PICO RIVERA CA 90660
1	UNITED DEFENSE LP PO BOX 359 D MARTIN SANTA CLARA CA 95052
1	UNITED DEFENSE LP PO BOX 58123 G THOMAS SANTA CLARA CA 95052
2	UNITED DEFENSE LP MAIL DROP M53 R BARRETT V HORVATICH 328 W BROKAW RD SANTA CLARA CA 95052-0359
3	UNITED DEFENSE LP GROUND SYSTEMS DIVISION M PEDRAZZI MAIL DROP N09 A LEE MAIL DROP N11 M MACLEAN MAIL DROP N06 1205 COLEMAN AVE SANTA CLARA CA 95052
4	UNITED DEFENSE LP 4800 EAST RIVER RD R BRYNSVOLD P JANKE MS170 T GIOVANETTI MS236 B VAN WYK MS389 MINNEAPOLIS MN 55421-1498

NO. OF COPIES	ORGANIZATION
2	GENERAL DYNAMICS LAND SYSTEMS D REES M PASIK PO BOX 2074 WARREN MI 48090-2074
1	GENERAL DYNAMICS LAND SYSTEMS DIVISION D BARTLE PO BOX 1901 WARREN MI 48090
1	GENERAL DYNAMICS LAND SYSTEMS MUSKEGON OPERATIONS W SOMMERS JR 76 GETTY ST MUSKEGON MI 49442
1	GENERAL DYNAMICS AMPHIBIOUS SYS SURVIVABILITY LEAD G WALKER 991 ANNAPOLIS WAY WOODBRIDGE VA 22191
5	INSTITUTE FOR ADVANCED TECH T KIEHNE H FAIR P SULLIVAN W REINECKE I MCNAB 4030 2 W BRAKER LN AUSTIN TX 78759
2	CIVIL ENGR RSCH FOUNDATION H BERNSTEIN PRESIDENT R BELLE 1015 15TH ST NW STE 600 WASHINGTON DC 20005
1	ARROW TECH ASSO 1233 SHELBURNE RD STE D 8 SOUTH BURLINGTON VT 05403-7700

NO. OF COPIES	ORGANIZATION
1	CONSULTANT R EICHELBERGER 409 W CATHERINE ST BEL AIR MD 21014-3613
1	UCLA MANE DEPT ENGR IV H THOMAS HAHN LOS ANGELES CA 90024-1597
2	U OF DAYTON RESEARCH INSTUTE RAN Y KIM AJIT K ROY 300 COLLEGE PARK AVE DAYTON OH 45469-0168
1	MIT P LAGACE 77 MASS AVE CAMBRIDGE MA 01887
1	IIT RESEARCH CENTER D ROSE 201 MILL ST ROME NY 13440-6916
1	GEORGIA TECH RESEARCH INSTITUTE GEORGIA INSTITUTE OF TECHNOLOGY P FRIEDERICH ATLANTA GA 30392
1	MICHIGAN ST UNIVERSITY R AVERILL 3515 EB MSM DEPT EAST LANSING MI 48824-1226
1	UNIVERSITY OF KENTUCKY LYNN PENN 763 ANDERSON HALL LEXINGTON KY 40506-0046
1	UNIVERSITY OF WYOMING D ADAMS PO BOX 3295 LARAMIE WY 82071

NO. OF COPIES	ORGANIZATION
1	UNIVERSITY OF UTAH DEPT OF MECH & INDUSTRIAL ENGR S SWANSON SALT LAKE CITY UT 84112
2	PENNSYLVANIA STATE UNIV R MCNITT C BAKIS 227 HAMMOND BLDG UNIVERSITY PARK PA 16802
1	PENNSYLVANIA STATE UNIV RENATA S ENGEL 245 HAMMOND BLDG UNIVERSITY PARK PA 16801
1	PURDUE UNIVERSITY SCHOOL OF AERO & ASTRO C T SUN W LAFAYETTE IN 47907-1282
1	STANFORD UNIVERSITY DEPARTMENT OF AERONAUTICS AND AEROBALLISTICS DURANT BUILDING S TSAI STANFORD CA 94305
1	UNIVERSITY OF DAYTON J M WHITNEY COLLEGE PARK AVE DAYTON OH 45469-0240
7	UNIVERSITY OF DELAWARE CTR FOR COMPOSITE MATERIALS J GILLESPIE M SANTARE G PALMESE S YARLAGADDA S ADVANI D HEIDER D KUKICH 201 SPENCER LABORATORY NEWARK DE 19716

NO. OF COPIES	ORGANIZATION
1	UNIVERSITY OF ILLINOIS AT URBANA CHAMPAIGN NATL CENTER FOR COMPOSITE MATERIALS RESEARCH 216 TALBOT LABORATORY J ECONOMY 104 S WRIGHT ST URBANA IL 61801
3	THE UNIVERSITY OF TEXAS AT AUSTIN CENTER FOR ELECTROMECHANICS J PRICE A WALLS J KITZMILLER 10100 BURNET RD AUSTIN TX 78758-4497
3	VA POLYTECHNICAL INSTITUTE & STATE UNIVERSITY DEPT OF ESM M W HYER K REIFSNIDER R JONES BLACKSBURG VA 24061-0219
1	NORTH CAROLINA STATE UNIVERSITY CIVIL ENGINEERING DEPT W RASDORF PO BOX 7908 RALEIGH NC 27696-7908
1	UNIVERSITY OF MARYLAND DEPT OF AEROSPACE ENGINEERING ANTHONY J VIZZINI COLLEGE PARK MD 20742
1	DREXEL UNIVERSITY ALBERT S D WANG 32ND AND CHESTNUT STREETS PHILADELPHIA PA 19104
1	SOUTHWEST RSCH INSTITUTE ENGR & MATL SCIENCES DIV J RIEGEL 6220 CULEBRA RD PO DRAWER 28510 SAN ANTONIO TX 78228-0510

NO. OF COPIES	ORGANIZATION
	ABERDEEN PROVING GROUND
1	COMMANDER US ARMY MATERIEL SYS ANALYSIS P DIETZ 392 HOPKINS RD AMXSY TD APG MD 21005-5071
1	DIRECTOR US ARMY RESEARCH LAB AMSRL OP AP L APG MD 21005 5066
115	DIR USARL AMSRL CI AMSRL CI H W STUREK AMSRL CI S A MARK AMSRL CS IO FI M ADAMSON AMSRL SL B J SMITH AMSRL SL BA AMSRL SL BL D BELY R HENRY AMSRL SL BG A YOUNG AMSRL SL I AMSRL WM B A HORST E SCHMIDT AMSRL WM BA W D AMICO F BRANDON AMSRL WM BC P PLOSTINS D LYON J NEWILL S WILKERSON A ZIELINSKI AMSRL WM BD B FORCH R FIFER R PESCE RODRIGUEZ B RICE

NO. OF COPIES	ORGANIZATION
	ABERDEEN PROVING GROUND (CONT)
	AMSRL WM BE G WREN C LEVERITT D KOOKER AMSRL WM BR C SHOEMAKER J BORNSTEIN AMSRL WM M D VIECHNICKI G HAGNAUER J MCCAULEY B TANNER AMSRL WM MA R SHUFORD P TOUCHET N BECK TAN D FLANAGAN L GHIORSE D HARRIS S MCKNIGHT P MOY S NGYUEN P PATTERSON G RODRIGUEZ A TEETS R YIN AMSRL WM MB B FINK J BENDER T BLANAS T BOGETTI R BOSSOLI L BURTON K BOYD S CORNELISON P DEHMER R DOOLEY W DRYSDALE G GAZONAS S GHIORSE D GRANVILLE D HOPKINS C HOPPEL D HENRY R KASTE M KLUSEWITZ M LEADORE R LIEB

NO. OF COPIES	ORGANIZATION
	ABERDEEN PROVING GROUND (CONT)
	AMSRL WM MB E RIGAS J SANDS D SPAGNUOLO W SPURGEON J TZENG E WETZEL A ABRAHAMIAN M BERMAN A FRYDMAN T LI W MCINTOSH E SZYMANSKI AMRSL WM MC J BEATTY J SWAB E CHIN J MONTGOMERY A WERESCZCAK J LASALVIA J WELLS AMSRL WM MD W ROY S WALSH AMSRL WM T B BURNS AMSRL WM TA W GILLICH T HAVEL J RUNYEON M BURKINS E HORWATH B GOOCH W BRUCHEY AMSRL WM TC R COATES AMSRL WM TD A DAS GUPTA T HADUCH T MOYNIHAN F GREGORY A RAJENDRAN M RAFTENBERG M BOTELER T WEERASOORIYA D DANDEKAR A DIETRICH

NO. OF
COPIES ORGANIZATION

ABERDEEN PROVING GROUND (CONT)

AMSRL WM TE
A NIILER
J POWELL
AMSRL SS SD
H WALLACE
AMSRL SS SE R
R CHASE
AMSRL SS SE DS
R REYZER
R ATKINSON
AMSRL SE L
R WEINRAUB
J DESMOND
D WOODBURY

NO. OF COPIES	ORGANIZATION
1	R MARTIN MERL LTD TAMWORTH RD HERTFORD SG13 7DG UK
1	PW LAY SMC SCOTLAND DERA ROSYTH ROSYTH ROYAL DOCKYARD DUNFERMLINE FIFE KY 11 2XR UK
1	T GOTTESMAN CIVIL AVIATION ADMINSTRATION PO BOX 8 BEN GURION INTERNL AIRPORT LOD 70150 ISRAEL
1	S ANDRE AEROSPATIALE A BTE CC RTE MD132 316 ROUTE DE BAYONNE TOULOUSE 31060 FRANCE
1	J BAUER DAIMLER BENZ AEROSPACE D 81663 MUNCHEN MUNICH GERMANY
3	DRA FORT HALSTEAD PETER N JONES DAVID SCOTT MIKE HINTON SEVEN OAKS KENT TN 147BP UNITED KINGDOM
1	MR FRANCOIS LESAGE DEFENSE RESEARCH ESTAB VALCARTIER PO BOX 8800 COURCELETTE QUEBEC COA IRO CANADA

NO. OF COPIES	ORGANIZATION
2	ROYAL MILITARY COLLEGE OF SCIENCE SHRIVENHAM D BULMAN B LAWTON SWINDON WILTS SN6 8LA UNITED KINGDOM
1	SWISS FEDERAL ARMAMENTS WKS WALTER LANZ ALLMENDSTRASSE 86 3602 THUN SWITZERLAND
1	PROFESSOR SOL BODNER ISRAEL INSTITUTE OF TECHNOLOGY FACULTY OF MECHANICAL ENGR HAIFA 3200 ISRAEL
1	DSTO MATERIALS RSRCH LAB DR NORBERT BURMAN NAVAL PLATFORM VULNERABILITY SHIP STRUCTURES & MATERIALS DIV PO BOX 50 ASCOT VALE VICTORIA AUSTRALIA 3032
1	PROFESSOR EDWARD CELENS ECOLE ROYAL MILITAIRE AVE DE LA RENAISSANCE 30 1040 BRUXELLE BELGIQUE
1	DEF RES ESTABLISHMENT VALCARTIER ALAIN DUPUIS 2459 BOULEVARD PIE XI NORTH VALCARTIER QUEBEC CANADA PO BOX 8800 COURCELETTE GOA IRO QUEBEC CANADA

NO. OF COPIES	ORGANIZATION
1	INSTITUT FRANCO ALLEMAND DE RECHERCHES DE SANIT LOUIS DE MARC GIRAUD RUE DU GENERAL CASSAGNOU BOITE POSTALE 34 F 68301 SAINT LOUIS CEDEX FRANCE
1	J MANSON ECOLE POLYTECH DMX LTC CH 1015 LAUSANNE SWITZERLAND
1	TNO PRINS MAURITS LAB DR ROB IJSSELSTEIN LANGE KLEIWEG 137 PO BOX 45 2280 AA RIJSWIJK THE NETHERLANDS
2	FOA NAT L DEFENSE RESEARCH ESTAB DR BO JANZON R HOLMLIN DIR DEPT OF WEAPONS & PROTECTION S 172 90 STOCKHOLM SWEDEN
2	DEFENSE TECH & PROC AGENCY GRND MR I CREWTHER GENERAL HERZOG HAUS 3602 THUN SWITZERLAND
1	MINISTRY OF DEFENCE RAFAEL DR MEIR MAYSELESS ARMAMENT DEVELOPMENT AUTH PO BOX 2250 HAIFA 31021 ISRAEL
1	DR AKE PERSSON DYNAMEC RESEARCH AB PARADISGRND 7 S 151 36 SODERTALJE SWEDEN

NO. OF COPIES	ORGANIZATION
1	ERNST MACH INSTITUT EMI DIRECTOR HAUPTSTRASSE 18 79576 WEIL AM RHEIN GERMANY
1	ERNST MACH INSTITUT EMI DR ALOIS STILP ECKERSTRASSE 4 7800 FREIBURG GERMANY
1	DR IR HANS PASMAN TNO DEFENSE RESEARCH POSTBUS 6006 2600 JA DELFT THE NETHERLANDS
1	DR BITAN HIRSCH TACHKEMONY ST 6 NETAMUA 42611 ISRAEL
1	PROF DR MANFRED HELD DEUTSCHE AEROSPACE AG DYNAMICS SYSTEMS PO BOX 1340 D 86523 SCHROBENHAUSEN GERMANY

REPORT DOCUMENTATION PAGE

Form Approved
OMB No. 0704-0188

1. AGENCY USE ONLY *(Leave blank)*	2. REPORT DATE	3. REPORT TYPE AND DATES COVERED
	June 2000	Final, December 1994 - March 1996

4. TITLE AND SUBTITLE
Induction Heating of Carbon-Fiber Composites: Experimental Verification of Models

5. FUNDING NUMBERS
AH42

6. AUTHOR(S)
Bruce K. Fink, Roy L. McCullough,* and John W. Gillespie, Jr.*

7. PERFORMING ORGANIZATION NAME(S) AND ADDRESS(ES)
U.S. Army Research Laboratory
ATTN: AMSRL-WM-MB
Aberdeen Proving Ground, MD 21005-5069

8. PERFORMING ORGANIZATION REPORT NUMBER
ARL-TR-2247

9. SPONSORING/MONITORING AGENCY NAMES(S) AND ADDRESS(ES)

10.SPONSORING/MONITORING AGENCY REPORT NUMBER

11. SUPPLEMENTARY NOTES
* University of Delaware, Newark, DE 19716

12a. DISTRIBUTION/AVAILABILITY STATEMENT
Approved for public release; distribution is unlimited.

12b. DISTRIBUTION CODE

13. ABSTRACT *(Maximum 200 words)*

Heating of continuous carbon-fiber-reinforced polymers (CFRP's) by the application of an alternating magnetic field has been shown to be due to dielectric losses in the polymer. Models that predict thermal generation in these composites are input to a finite element heat-transfer analysis, providing the predicted transient thermal profile in the plane of the laminate. The validity of the global thermal generation model is established through an experimental test matrix in which various specimen configurations are evaluated and compared with theoretical predictions of transient surface temperatures.

14. SUBJECT TERMS
carbon fiber, composites, induction heating, dielectric properties

15. NUMBER OF PAGES
64

16. PRICE CODE

17. SECURITY CLASSIFICATION OF REPORT	18. SECURITY CLASSIFICATION OF THIS PAGE	19. SECURITY CLASSIFICATION OF ABSTRACT	20. LIMITATION OF ABSTRACT
UNCLASSIFIED	UNCLASSIFIED	UNCLASSIFIED	UNCLASSIFIED

NSN 7540-01-280-5500

Standard Form 298 (Rev. 2-89)
Prescribed by ANSI Std. 239-18 298-102

INTENTIONALLY LEFT BLANK.

USER EVALUATION SHEET/CHANGE OF ADDRESS

This Laboratory undertakes a continuing effort to improve the quality of the reports it publishes. Your comments/answers to the items/questions below will aid us in our efforts.

1. ARL Report Number/Author ARL-TR-2247 (Fink) Date of Report June 2000

2. Date Report Received ______

3. Does this report satisfy a need? (Comment on purpose, related project, or other area of interest for which the report will be used.) ______

4. Specifically, how is the report being used? (Information source, design data, procedure, source of ideas, etc.) ______

5. Has the information in this report led to any quantitative savings as far as man-hours or dollars saved, operating costs avoided, or efficiencies achieved, etc? If so, please elaborate. ______

6. General Comments. What do you think should be changed to improve future reports? (Indicate changes to organization, technical content, format, etc.) ______

CURRENT ADDRESS

Organization

Name E-mail Name

Street or P.O. Box No.

City, State, Zip Code

7. If indicating a Change of Address or Address Correction, please provide the Current or Correct address above and the Old or Incorrect address below.

OLD ADDRESS

Organization

Name

Street or P.O. Box No.

City, State, Zip Code

(Remove this sheet, fold as indicated, tape closed, and mail.)

(DO NOT STAPLE)